DEVELOPING A HIGH SENSITIVITY AND SPATIAL RESOLUTION SPECT MOLECULAR IMAGING SYSTEM THROUGH THE USE OF NOVEL MULTIPLEXING

By

Oleg Sergeevich Ovchinnikov

Thesis

Submitted to the Faculty of the

Graduate School of Vanderbilt University

in partial fulfillment of requirements

for the degree of

MASTER OF SCIENCE

in

Physics

August, 2014

Nashville, Tennessee

Approved:

Todd E. Peterson, Ph.D.

A. S. Umar Ph.D.

To my mother and father, Alexandra and Serge Ovchinnikov, for all their support

TABLE OF CONTENTS

Page

LIST OF TABLES

Table Page

LIST OF FIGURES

Figure Page

LIST OF ABBREVIATIONS

SPECT - Single Photon Emitted Computational Tomography

PET - Positron Emission Tomography

MRI - Magnetic Resonance Imaging

HPGe - High Purity Germanium

Si – Silicon

eV – electron volts

DSSD - Double Sided Strip Detector

OSEM - Ordered subset expectation maximization

MLEM – Maximum likelihood expectation maximization

LSQ - Least Squares

PCA - Principle Component Analysis

^{57}Co – Cobalt-57

^{123}I - Iodine-123

Ci - curie

CHAPTER I

INTRODUCTION

Molecular imaging is an important tool in both clinical and preclinical settings [1]. Molecular imaging consists of many different modalities which include Magnetic Resonance Imaging (MRI), Positron Emission Tomography (PET), Single Photon Emission Computed Tomography (SPECT), and many others. These techniques provide important information for everything from medical diagnoses in the hospital to looking at the spatial distribution of drugs in the body. Each of these modalities has benefits and shortcomings that are unique to the system. Overcoming the shortcomings of each modality is a large and active area of research. SPECT works through the use of a radiotracer. In the case of SPECT, this is a gamma emitter attached to a molecule whose spatial distribution in the object will be measured. A shortcoming of SPECT arises from the need to use collimation, required in SPECT imaging in order to achieve any information of ordination of photon, in conjunction with the gamma emitter. Collimation greatly reduces the sensitivity of the system since a large majority of the emitted photons never reach the detector. This is especially true for pinhole collimation where every voxel in space has very limited angle from which emitted photon can interact with the detector (Figure 1).

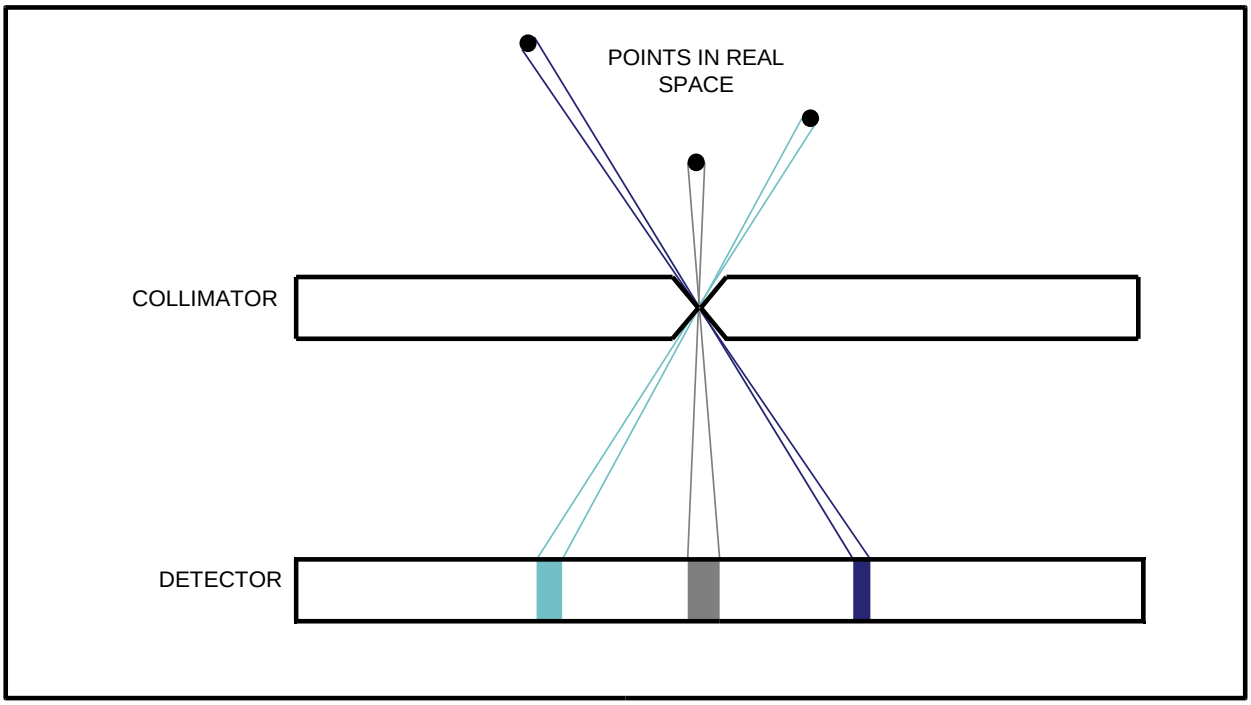

Figure 1. Single pinhole collimation

The use of a clever collimation design can offer potential solutions. However, capitalizing on the advantages requires advances in signal acquisition methodologies.

The need for better analytical tools that can provide high sensitivity, detailed molecular information with high spatial resolution is well recognized and is evidenced by the fact that it is a goal sought by many researchers and the impetus behind the development of several different molecular imaging techniques. Preclinical SPECT systems have advanced much over the years. Many early preclinical SPECT systems relied on single pinhole collimators [4-7]. These systems required extremely long acquisitions and high radiation doses for the subject. Newer preclinical systems generally rely on multi-pinhole collimators [8-13] (Figure 2).

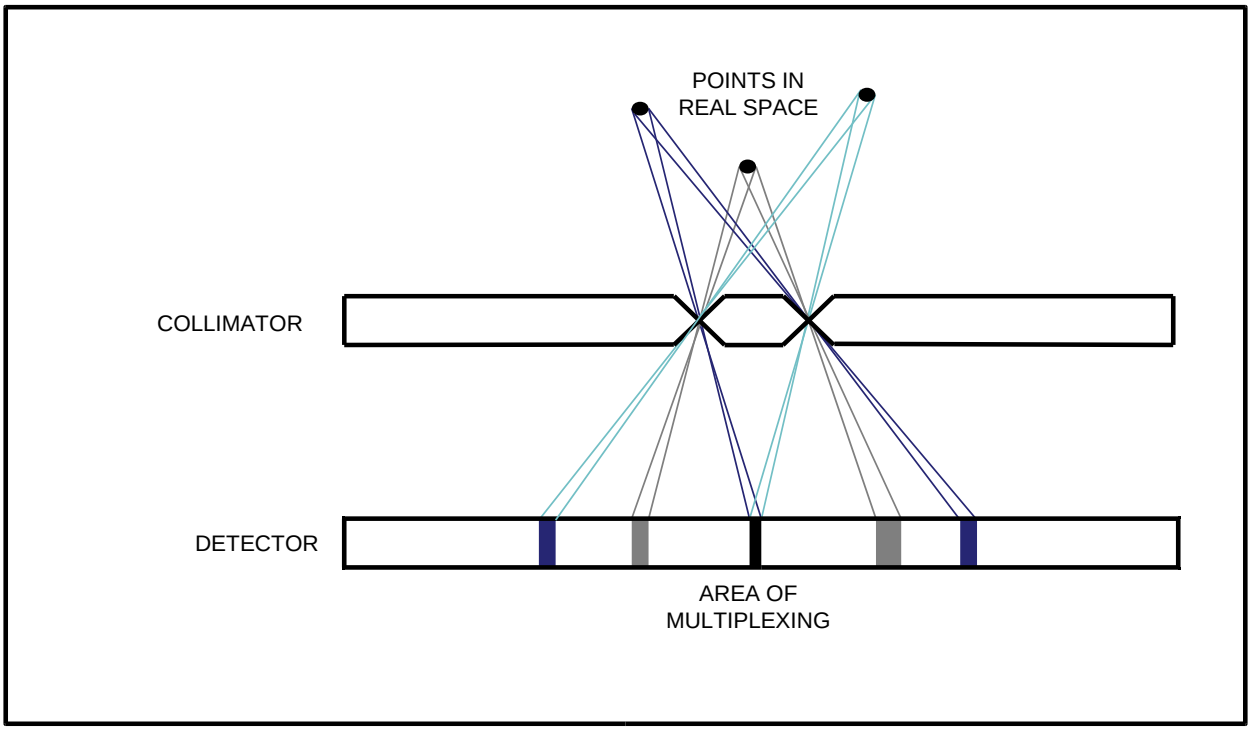

Figure 2. Multi-pinhole collimation

These systems benefit from both a reduction in scan time and required radiation dose compared to older single pinhole systems. Many different preclinical SPECT system designs utilize multi-pinhole collimation including A-SPECT, HiSPECT, U-SPECT, T-SPECT, Mirco-SPECT, SemiSPECT, X-SPECT, and FAST-SPECT, along with many others [6-18]. However, with multi-pinhole SPECT arises the problem of multiplexing, or the inability to tell through which pinhole a photon passed. Multiplexing allows for an increase in sensitivity; however it comes with the problem that it leads to artifacts during image reconstruction [32-34]. Due to this problem most systems try to limit the amount of multiplexing that is present. One potential solution to this is synthetic collimation, using two magnifications to remove artifacts in image reconstruction caused by only having one (Figure 3). Most modern systems rely on standard pixel detectors that utilize

photomultiplier tubes in order to detect photon interactions; many modern systems utilize detectors such as sodium iodide, which have energy resolutions in the range of 10% FWHM at 140 keV [6-18]. Even many systems that utilize more high-resolution detectors utilize detectors such as CZT, which has an energy resolution of around 5%. These energy resolutions make it difficult in many instances to perform multi-isotope studies on two isotopes that have relatively close energies due to the inability to distinguish from which isotope a photon originated. However, even with these limitations, the use of these types of systems is invaluable in many areas of preclinical imaging. SPECT imaging is used in all manner of studies including cardiovascular imaging, bone metabolism, and neuroimaging [20-27].

Through the use of a stacked array of detectors as shown in figure 3, it is possible to overcome the traditional trade-off in collimator design of high resolution vs. high sensitivity. This is done by allowing the back detector, farthest form entrance window, to have a high degree of multiplexing, while using the information in the second detector in the stacked array to remove any artifact that might appear in the reconstruction from a high degree of multiplexing.

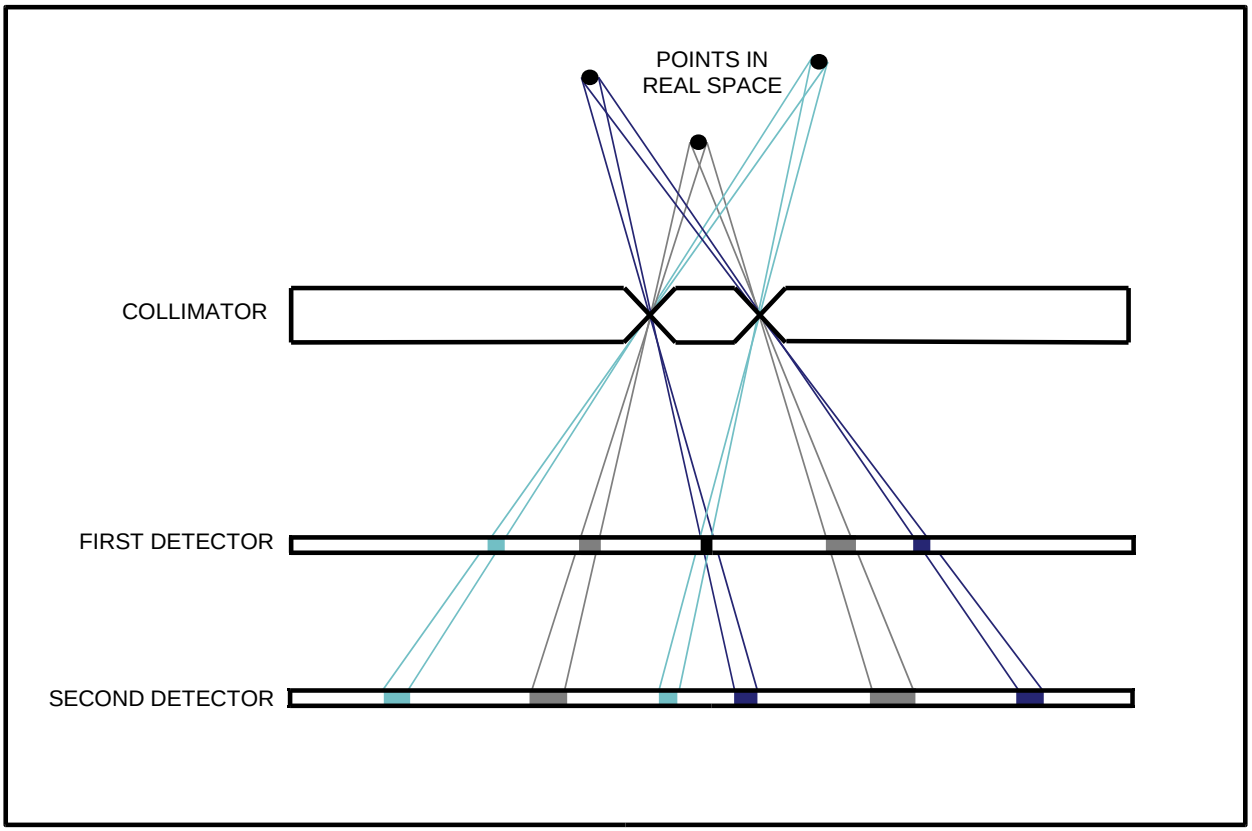

Figure 3. Multi-pinhole collimation with synthetic collimation

This will also allow for the use of both high magnification and low magnification information at the same time, allowing for more information about the trajectories of the photons. Through the use of different materials for the front and back detectors in the detector array it is also possible to obtain beneficial properties of both detector types. These benefits include the extremely high spatial resolution of the silicon detector as well as the high energy resolution of the High Purity Germanium Detector allowing for multi-isotope imaging as well as a high degree of scatter rejection. Not only do we achieve the benefits of the different types of detectors but it is also possible to mitigate if not remove the shortcomings of each detector through the use of the two detector setup and by having a small imaging field of view. The small imaging field of view of the

system limits the studies that can be done with such a system; however the combination of high spatial resolution and sensitivity lends itself well to preclinical imaging where this small field of view will not be a problem. One of the regions in preclinical imaging that could see a real benefit from the combination of high spatial resolution and high sensitivity is mouse brain imaging. With a need to track even the smallest concentrations and the ability for high spatial localization, mouse brain imaging presents a perfect area of study to test and optimize the abilities of a stacked detector array imaging system.

The objective of the Masters thesis is to design and construct a dedicated synthetic collimation camera to be utilized in a future SPECT system. The work will focus on the preparation of the detectors for use in SPECT imaging, the design of the camera housing for the detectors for them to operate in parallel, and initial demonstration of the camera's imaging capability. Finally, a method for designing a multi-pinhole collimator will also be presented.

CHAPTER II

HPGe DETECTOR FOR IMAGING

High Purity Germanium (HPGe) Detectors have been used in many areas of science for decades and are known for their excellent energy resolution. HPGe detectors have many properties that make them a desired detector in many applications; their excellent energy resolution, stopping power, and large energy range are just a few such properties. They however have required bulky cooling systems that have limited their usefulness in many areas of research where space and weight are a concern. Recent technological advances have allowed for the shrinkage of these cooling systems from bulky large liquid nitrogen dewars to small mechanical cooling systems (Figure 4). These cooling systems can be assembled in many different configurations depending on the application allowing for more flexibility.

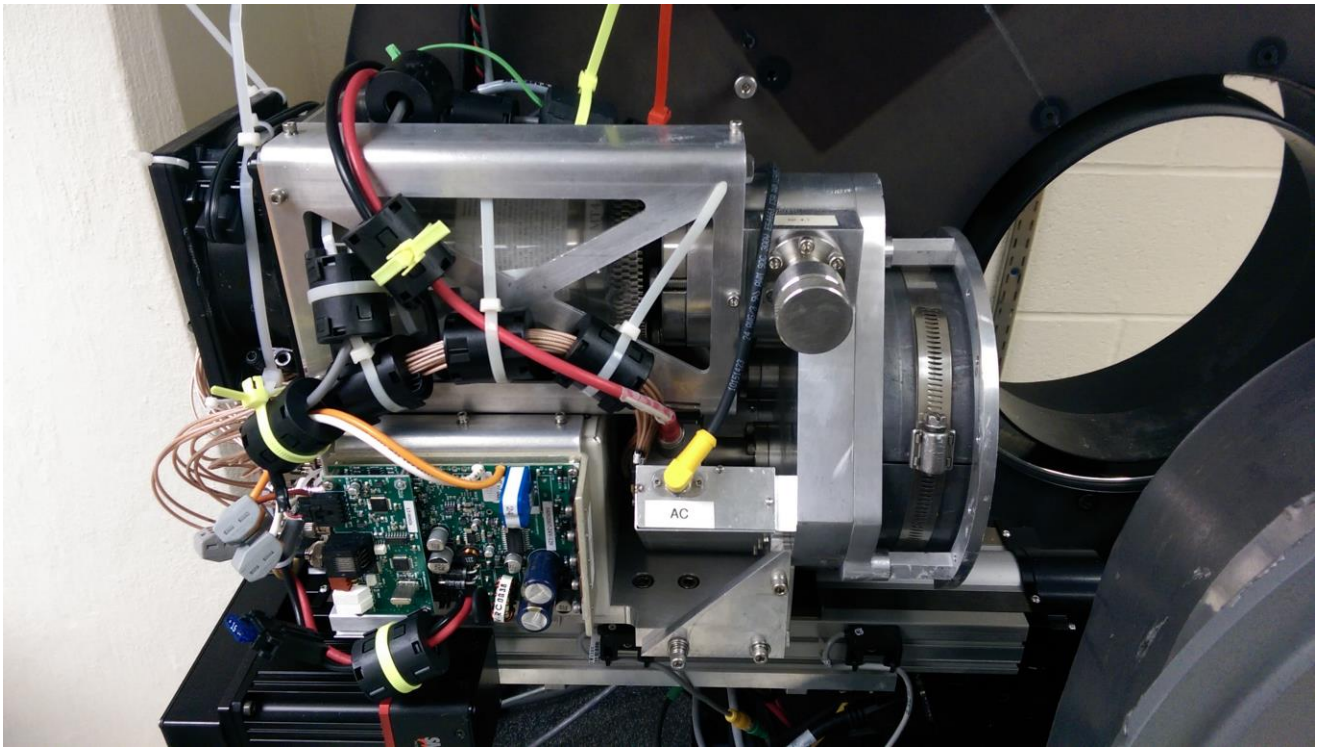

Figure 4. HPGe detector with mechanical cooling behind the detector

These advances have allowed for these detectors to be utilized in many fields that would not have been able to use them due to the cooling requirements. One field that could benefit from the properties of HPGe detectors is clinical / preclinical imaging. Their high energy resolution can be utilized for scatter rejection and multi-isotope imaging. Clinical imaging in particular with its much larger size of imaging subjects could benefit from these properties of scatter rejection to achieve better image reconstruction.

To show the benefits of these detectors in clinical/preclinical imaging we constructed and tested a SPECT system that utilizes HPGe detectors. We utilized a HPGe detector developed by PHDS Co. based in Knoxville, TN. These detectors are

Double Sided Strip Detectors (DSSD) with 16 by 16 orthogonal strips and are mechanically cooled to below 80K (Figure 5).

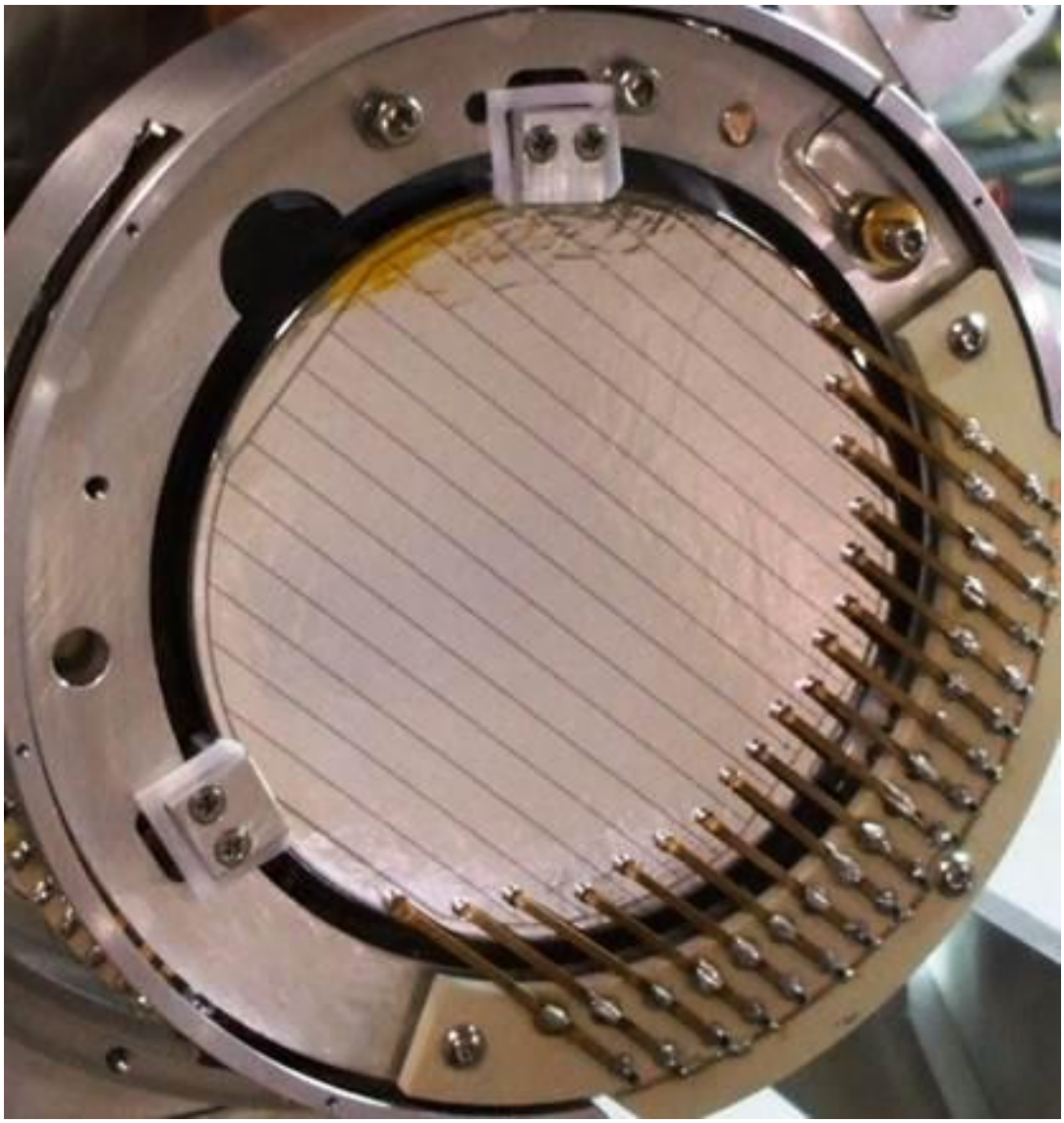

Figure 5. HPGe detector crystal showing 16 strips

The detectors utilize sub-strip interpolation to achieve higher spatial resolution than the strip width would allow. The iteration of HPGe detectors that are utilized in this system

are ideal for preclinical imaging. However, due to their limited detection area they are not suitable for clinical imaging (Table 1).

	Germanium
Strip Pitch	5 mm
Detector Thickness	10 mm
Spatial Resolution	1.5 mm
Active Area	55 cm2
Energy Range	>~60 keV

Table 1. HPGe detector parameters

The imaging system utilized a single pinhole collimator to not introduce compounding factors such as multiplexing into testing of the imaging system. Software was developed that would allow for precise control of the detector and multiple motors for translation and rotation of objects in front of the detector [58].

To test the imaging properties of the system we required a method of reconstructing the projections collected by the system into a reconstructed image. We decided to look at the performance of both Ordered Subset Expectation Maximization (OSEM) and Maximum Likelihood Expectation Maximization (MLEM) [59-63]. Both of these reconstruction methods try to iteratively solve the projection equation which requires prior knowledge of the H-matrix, information on how every voxel in object space projects into detector space. This matrix is from the projection equation g=H*f+n where g is the projection on to the detector, f is the distribution of radiotracer, what is being projected, in the object and n is the noise. An H-Matrix can be acquired in one of

two main ways: experimentally or analytically. An experimental H-matrix is acquired by moving a point source through every voxel in object space and storing the associated projections into detector space. This method is extremely time consuming; however, it is the best realization of the H-matrix since it includes all aspects of the system's performance, such as pinhole penetration, scatter inside the detector, and depth of interaction effects, just to name a few. An analytical H-matrix is achieved by parameterizing the response of the detector with a mathematical function of how the collimator should project the object onto the detector. This method is much quicker; however it does not have as much information on the system.

Both of these methods have advantages and disadvantages associated with them. For initial testing we decided to focus on using an experimentally acquired system matrix, since it would present the most complete representation of the H-matrix we could obtain. We obtained this H-matrix by moving a Co-57 point source through every voxel in image space. Even at a lower resolution than desired this requires a large amount of time. The H-matrix that was collected was of an object space of $40x40x40mm^3$ with 1mm voxels and required 64000 points. This was done by attaching a Co-57 point source to the 3-axis translation stage and stepping through all x,y,z coordinates of the 64000 points, requiring multiple days of collection made possible by the half-life, 271 days, of Co-57. For the same object space with resolution of 0.5 mm would require 512000 points. This makes collecting every single point in space unfeasible for large high resolution object spaces.

CHAPTER III

INTERPOLATION OF EXPERIMENTAL H-MATRIX

Collection of an experimentally acquired H-matrix is desired proposition for testing reconstruction on a SPECT system. Experimentally acquired H-matrices contain all information about the system allowing for better image reconstruction and do not require any foreknowledge of the response of the system. However, the collection of an experimental H-matrix is an extremely lengthy procedure, for a large high resolution object space it requires an unfeasibly long period of time. This problem is extremely concerning in any imaging method that uses a decaying signal such as SPECT since time is limited. To use an experimentally acquired H-matrix in image reconstruction requires a method of speeding up the collection. One possible method is to collect at lower resolution and then to interpolate this data. This method allows for the collection of a high spatial resolution experimental H-matrix in a fraction of the time. The method has two primary limitations, the first being the parameterization of the H-matrix, and the second being how to achieve the interpolation of that parameterized H-matrix.

The need to parameterize the H-matrix is not strictly necessary since one could interpolate the detector response functions directly, but this is not ideal for a number of reasons. The first being noise, since the amount of points needed for even the low resolution collection is staggering, the time spent at any single point is minimized. This leads to a certain amount of noise in the projection. Parameterization should remove this noise and make it so that this noise does not propagate in the interpolation. Parameterization also allows for the storing of large amounts of data in a fraction of the

space, this can be important since even low resolution H-matrices can be in the multiple gigabytes in size. By parameterization the size of the data is reduced by orders of magnitude allowing for storage of many data sets with out worry. Parameterization also simplifies the interpolation process since it reduces the data into a clean set of hopefully independent parameters.

The method of parameterization presents a challenge since it is not clear how to approach this. The most straightforward method would be to parameterize the detector response at each voxel; however it is just as possible to parameterize the object space from the view of the detector. Parameterization of the detector response is the method we chose to pursue since this method allows to parameterize a 2d projection instead of a 3d space. Along with 2d vs. 3d space this is a much more straightforward problem since how a point source projects through a pinhole onto a detector is highly studied. Two methods of parameterization were looked at, with both offering advantages and disadvantages.

For the first attempt at this the detector response was assumed to be a Gaussian distribution and each response function was fit to a 2d Gaussian though a least squares (LSQ) non-linear fit. Other distributions also were examined such as the Cauchy distribution; however the Gaussian tended to give the most uniform results across a large amount of point source projections. While other distributions, such as lorentzian in highly off axis cases, gave less error than the Gaussian in certain cases, it preformed the best overall and was chosen as the fitting function to parameterize the H-matrix. An advantage of this is that the fit takes a projection of 160X160 pixels and outputs 5 values, each with a known effect. The five parameters in the case of the Gaussian

function are amplitude, x and y center position, and x and y widths. This allows for much easier and straightforward interpolation of these values than of the full 160X160X10 response. The fitting showed overall good fitting, with best results when the fit was implemented on all detector depths summed together vs. when each depth was fitted separately, this is because of a low amount of counts on many levels (Figure 6).

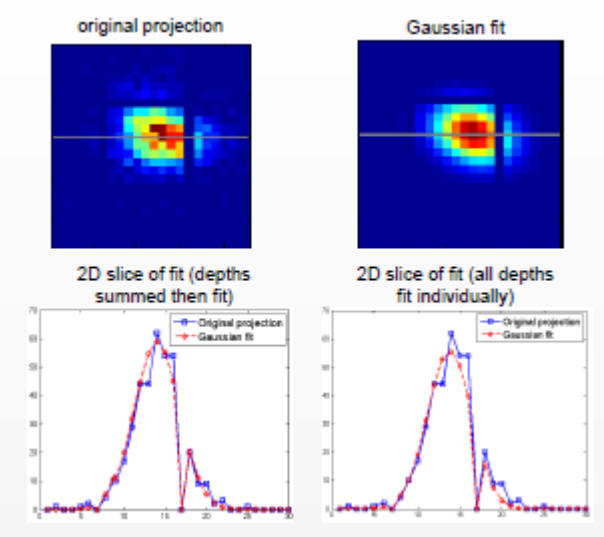

Figure 6. Example of a projection vs. fitted projections

The second method that was investigated was the use of Principle Component Analysis (PCA). PCA takes the response functions and deconvolves them into a series of eigenvalues and eigenvectors. The eigenvectors represent the orthogonal components that are common to the detector response functions. This method does not require any foreknowledge of the response function and as such is not limited by preconceived notions. This method also breaks the responses into a series of eigenvectors of which only the first few contain the majority of the information, allowing the H-matrix to be parameterized using only a few eigenvectors and corresponding eigenvalues for each

voxel. While a few eigenvectors do contain most of the information, they also have no physical meaning and when removing eigenvectors with little information it is possible to remove high frequency parts of the response that can be important. The main reason PCA was not chosen was inconsistence in how the eigenvalues would interpolate. In certain cases PCA worked much worse than Gaussian fit interpolation, which might be a problem with the type of interpolation we used, linear, and could have been solved through the use of a different interpolation method, or it could be a problem of missing information from lower information eigenvectors. Due this it was not pursued any further as a potential method.

Once the response was parameterized the next step was interpolation. This was done by initially using a linear interpolation that utilized nearest neighbors. To test the interpolation method a collected H-matrix was taken and had its resolution cut in half (half of the points removed) and then was interpolated back to full. This allowed us to look at the agreement between interpolated and collected, and if the error was within acceptable amounts. The interpolation was performed on the function parameterized values, and the interpolation had some problems with the angle. The problem with the angle was solved by limiting the angle to only a few quadrants, once this problem was solved the resulting interpolation was not perfect but within an acceptable amount of error, only a few percent or less, for us to continue. The effects of this error are slightly noticeable in the reconstructed image but only in the spill over from the center of the point source into neighboring voxels (Figure 7).

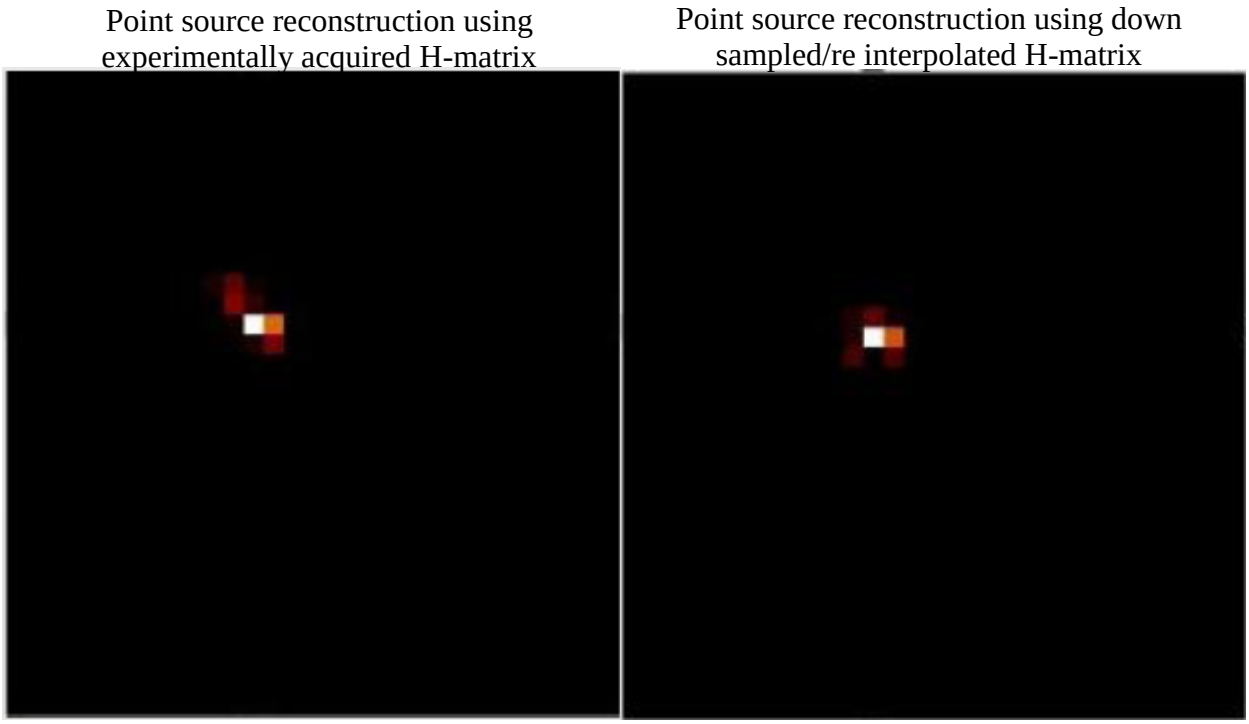

Figure 7. Reconstruction with original collected H-matrix vs using down sampled/re interpolated H-matrix

The interpolation of the data to higher resolution will have less error since the distance between points is smaller than in the test case. Along with linear nearest neighbor interpolation many other options were attempted to achieve better results, but all were worse or only marginally better. Once this higher resolution H-matrix was achieved it was possible for us to test the image reconstruction of HPGe imaging system. For reconstruction we were able to take an H-matrix collected at 1mm spatial resolution and interpolate down to 1/3mm resolution, however this proved problematic due to low sensitively per voxel and intrinsic resolution of detector. For most reconstructions a resolution of 0.5mm was utilized since it showed the most benefit of all resolutions tested. The improvement from this interpolation is easily noticeable in the reconstruction

of a point source using the original resolution and higher resolution H-matrix (Figure 8) [58].

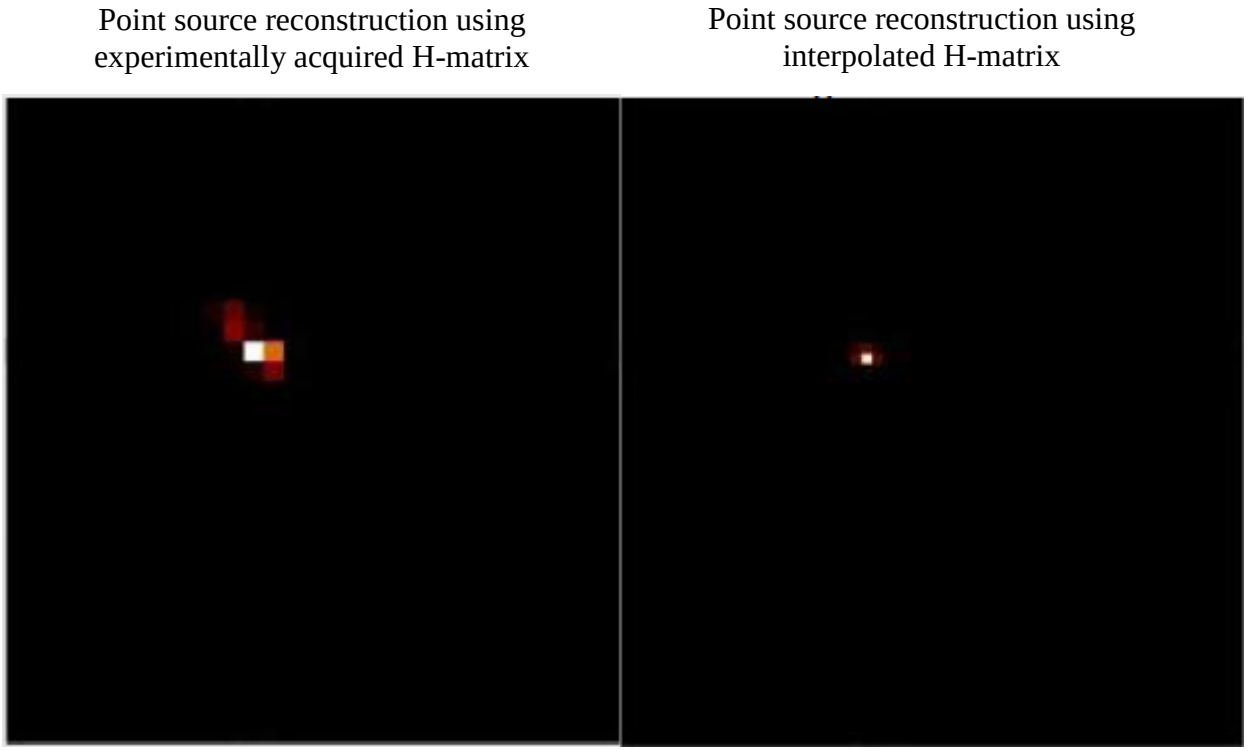

Figure 8. Reconstruction with original collected H-matrix vs. H-matrix interpolated to 0.5mm resolution

CHAPTER IV

DESIGN OF HOUSING FOR SILICON DETECTOR

Once imaging was possible with an HPGe imaging system, attention turned to attaching a silicon (Si) detector in front of the HPGE to create a stacked detector camera that images at different magnifications simultaneously. A camera setup with a Si detector in front of an HPGe detector represents a new and interesting development in SPECT imaging. This camera set up would be an improvement over current synthetic multiplexing camera designs. The reason for this is that the two detectors image over different energy ranges. While the Si detector images at lower energies, below 60 keV, while HPGe images at energy ranges above that.

	Silicon
Strip Pitch	59 μm
Detector Thickness	1 mm
Spatial Resolution	59 μm
Active Area	36.5 cm2
Energy Range	< 60 keV

Table 2. Si Detector parameters

This is important since if the two would image at the same energy range the first one would stop a majority of the photons, meaning that the sensitivity of the second would be extremely low. The fact that the two detectors operate over different energy ranges

means that you would have to image with labeled with a radio-isotope that emits at both energies. One such isotope is Iodine-123 (^{123}I). ^{123}I emits at both ~30 keV and 159 keV, allowing both detectors to operate in their preferred energy range. With the much higher energy 159 keV photon the silicon detector has minimum interaction and does not interfere with the HPGe image.

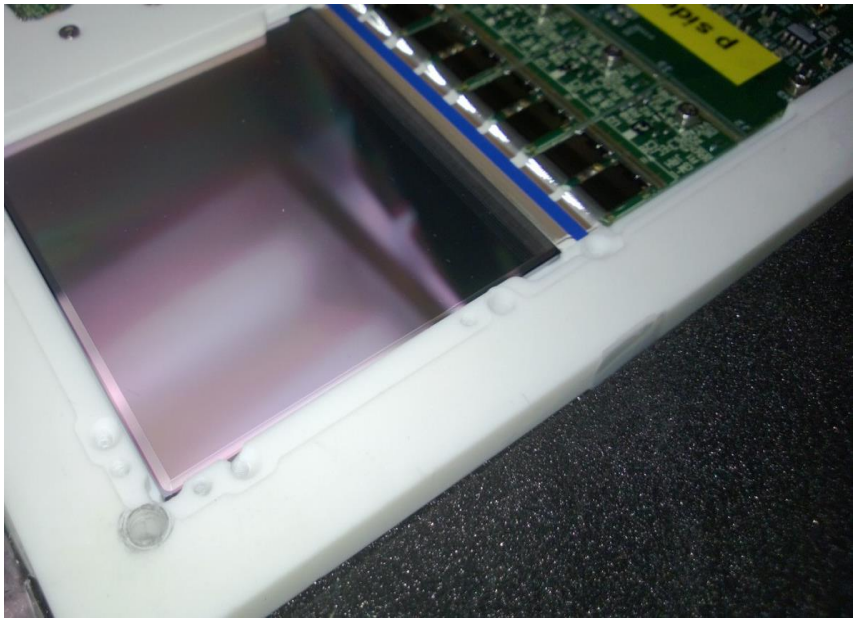

Figure 9. Si detector active area showing1024 strips

The Si detectors that were utilized in the camera construction consisted of DSSDs with 1024 by 1024 strips with a 59 μm strip pitch (Table 2 and Figure 9), allowing for much higher spatial resolution than the HPGe detector. The Si having a smaller active area is not of concern since it will be positioned closer to the pinhole collimator.

The HPGe detectors have a mounting ring onto which we can install the Si detector. While the HPGe requires that the detector be in a vacuum and is mechanically cooled, the requirements of the Si detector are much simpler. The Si detector when

operational must be in a light tight container and for stable operation must be kept at a constant temperature. To achieve this we decided to use the shell of the housing enclosure for the Si detector as a heat sink (Figure 10). This allows the Si detector to maintain a constant temperature without the need for external cooling, which could interfere with the light tight nature of the enclosure. The Si detector was situated at the side of the enclosure that is farthest from the HPGe Detector. The reason for this is that the heat sink of the Si detector not be directed into the face of the HPGe detector as well as the fact that the larger the difference in magnification of the two detectors, the better for the design of this system. The focal lengths with a closely placed pinhole, an important factor in the calculation magnification, are 78 mm for HPGe and 37 mm for Si.

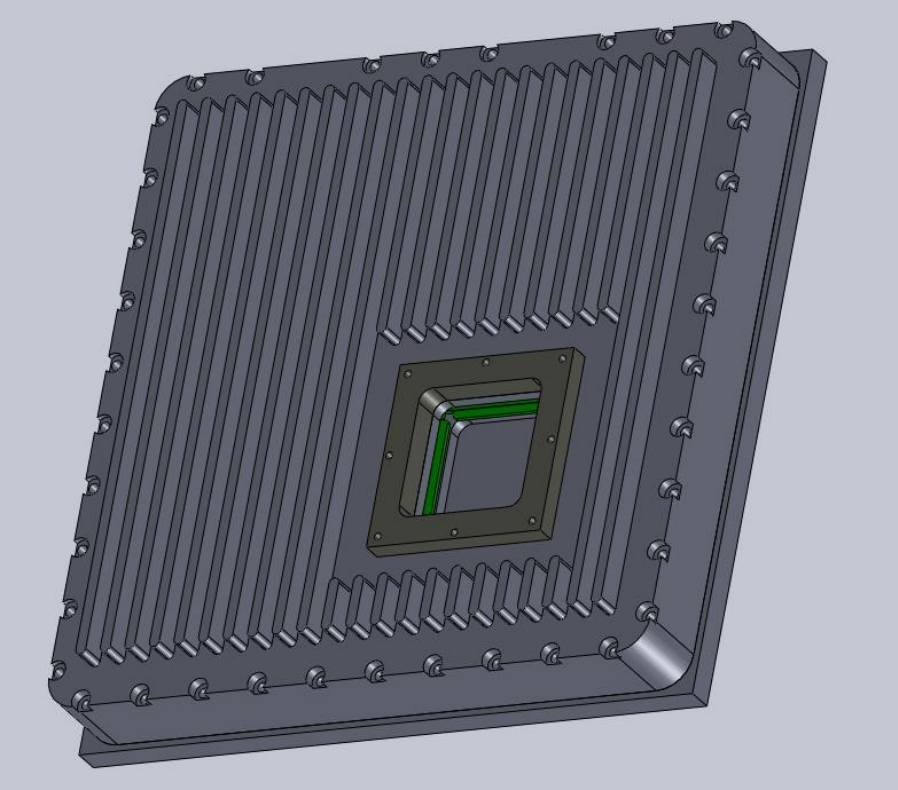

Figure 10. 3D model of Si enclosure front with cooling fins

The housing of the Si consists of two pieces of aluminum and an aluminum mounting bracket for the collimator. The collimator mounting was designed as a separate piece to allow for use of different collimators, with different mounting techniques, in the future. The front, farthest from the HPGE detector, holds the Si detector and has an opening window in it the size of the Si detector's active area (Figure 11). This opening was covered with a piece of thin translucent polycarbonate material for the housing to be light tight while keeping the attenuation to a minimum.

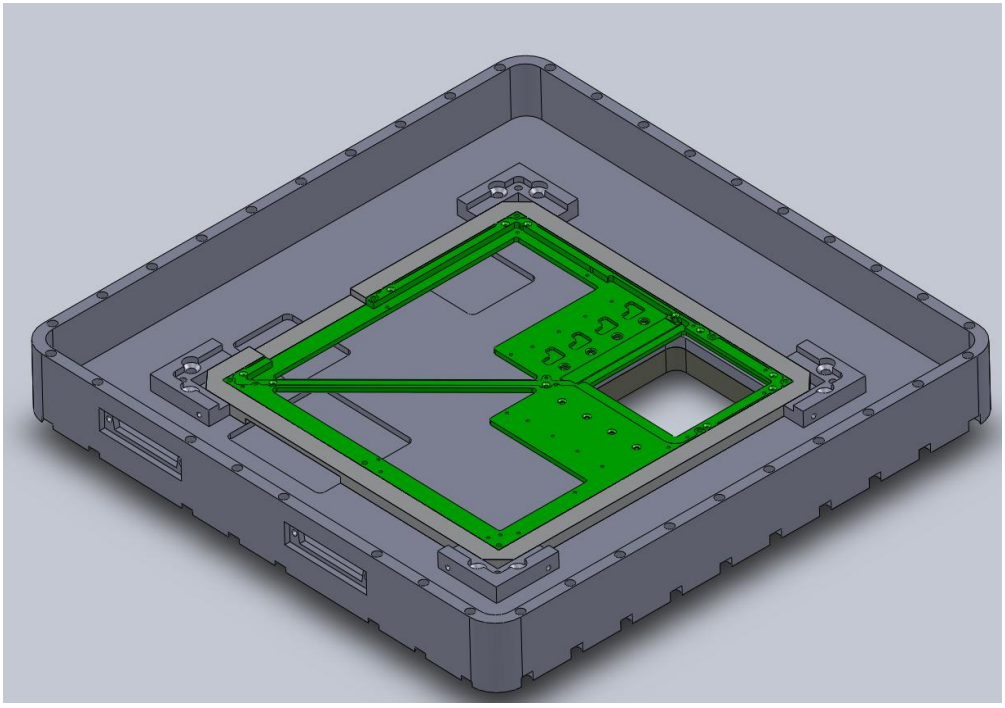

Figure 11. 3D model of Si enclosure front

The rear, closest to HPGe, has a very thin aluminum exit window, only a few thousandths of an inch thick (Figure 12). Aluminum over the same material as the HPGe entrance window was chosen since it is part of the housing, minimizing locations

for light leaks along with the fact that the higher operational energy range of the HPGe detector means that the extra material will have minimal effect on image quality.

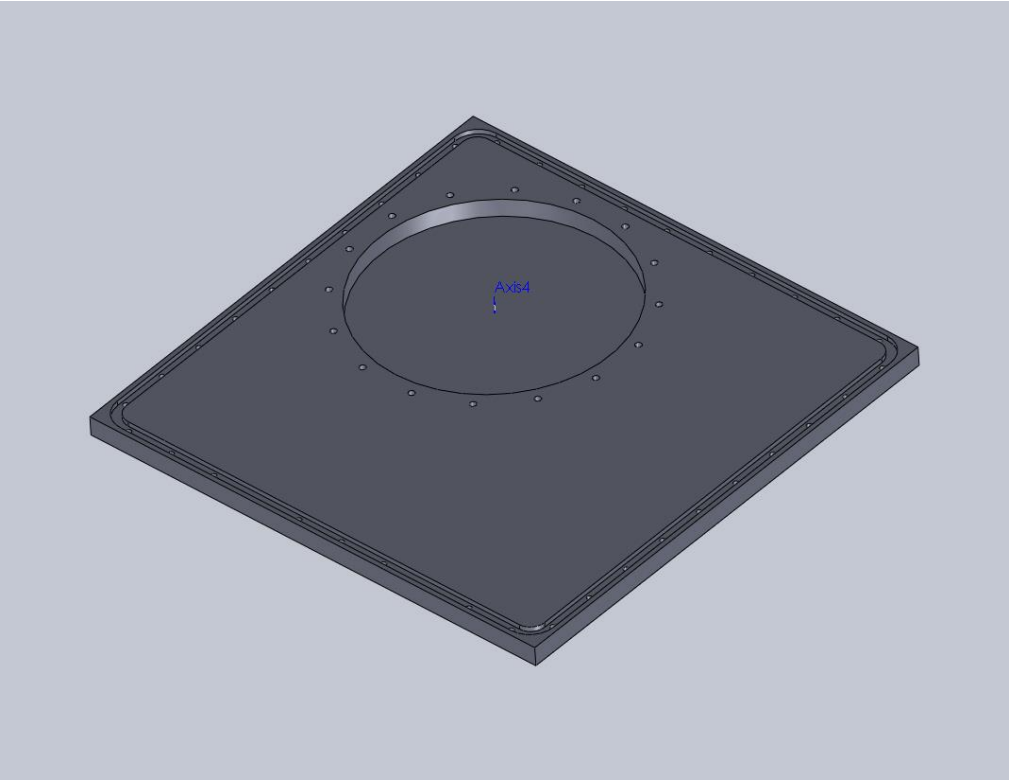

Figure 12. 3D model of Si enclosure back

Testing of this housing has shown that this is indeed the case that the extra material has a minimum effect on the energy spectrum of the HPGe detector. This was tested through the use of a ^{57}Co point source at a large distance away from the detector to produce a uniform flood and looking at the effect of the housing on the energy spectrum (Figure 13).

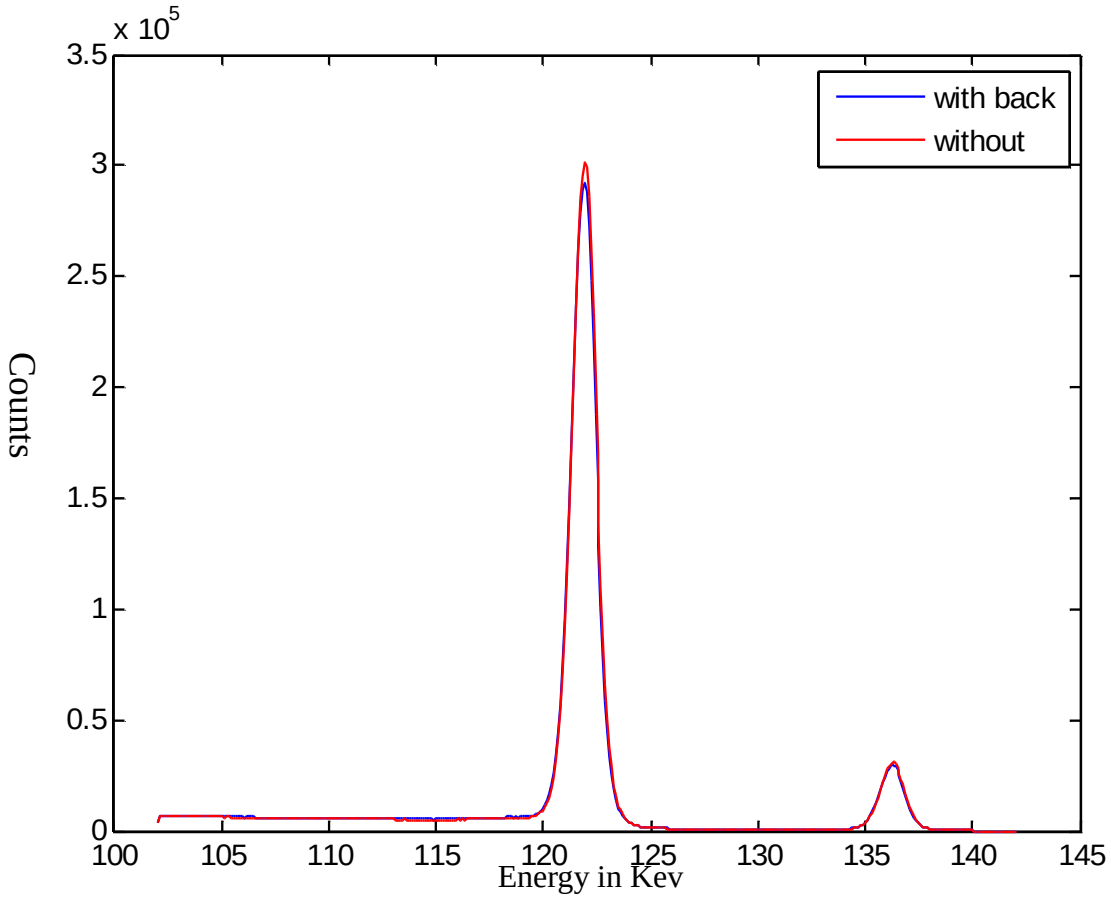

Figure 13. Effect of back of box on HPGe Spectrum

The housing is not thick enough to stop many high energy photons, <1% are attenuated, it is however thick enough that it will stop any low energy photons that would interact with the silicon detector. The main body on the other hand would ideally stop all high energy photons; the thickness of the housing means that a majority of the photons (~85%) are attenuated. One noticeable effect of the box, in the collected spectra on the HPGe detector, is the large amount of down scatter it produced (Figure 14). This is easily solved by placing a thin amount shielding between the object space and the Si enclosure, or through the use of the excellent energy resolution of the HPGe

detector. In most cases the collimator, designed to stop high energy photons, is large enough to accomplish this. The design of the Si detector housing allows for the mounting of a Si detector onto the front of an HPGe detector with little to no effect of the imaging quality of the HPGe detector.

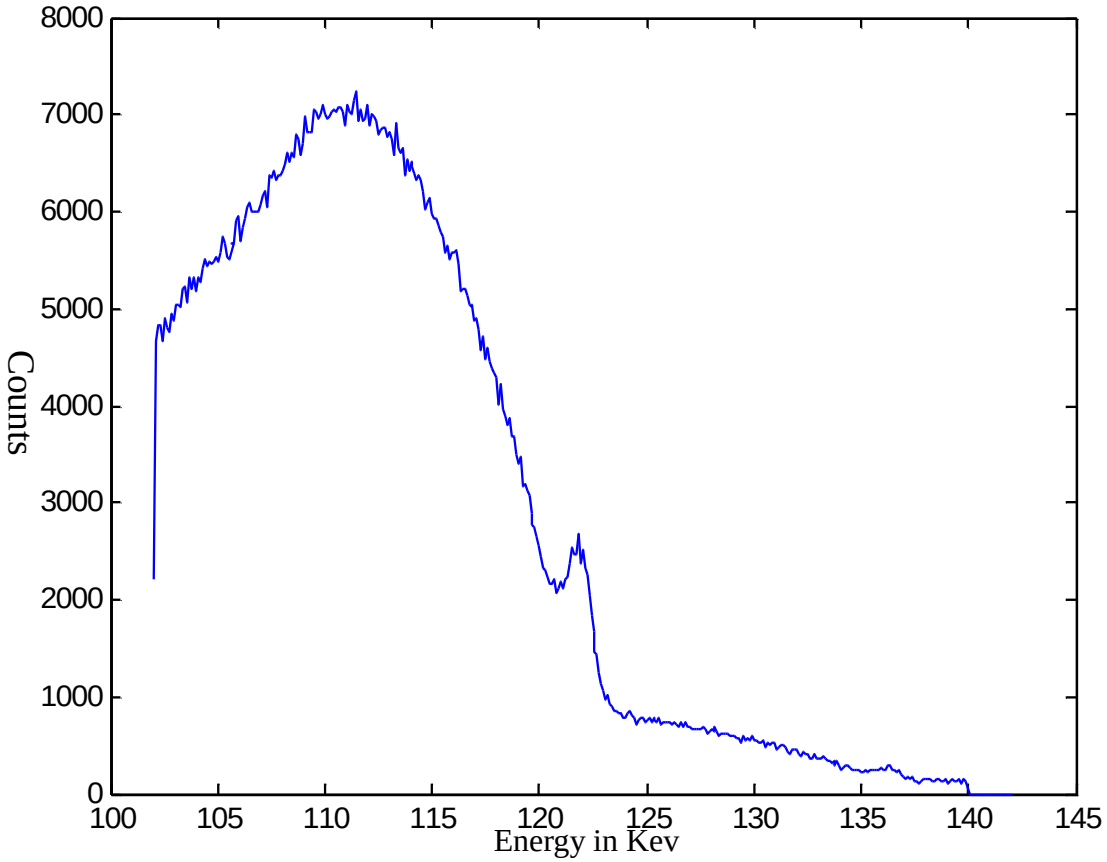

Figure 14. HPGe Spectrum pinhole collimator point source at extremely far away to show scatter due to box

.

CHAPTER V

SILICON DETECTOR UNIFORMITY

The Si detectors we are utilizing are DSSD slike the HPGe detectors, they however do not use any form of sub-strip interpolation. Each detector side has 8 readout chips and 128 strips per chip. A large problem that has been encountered when working with the Si detectors is that the response across them is not uniform (Figure 15).

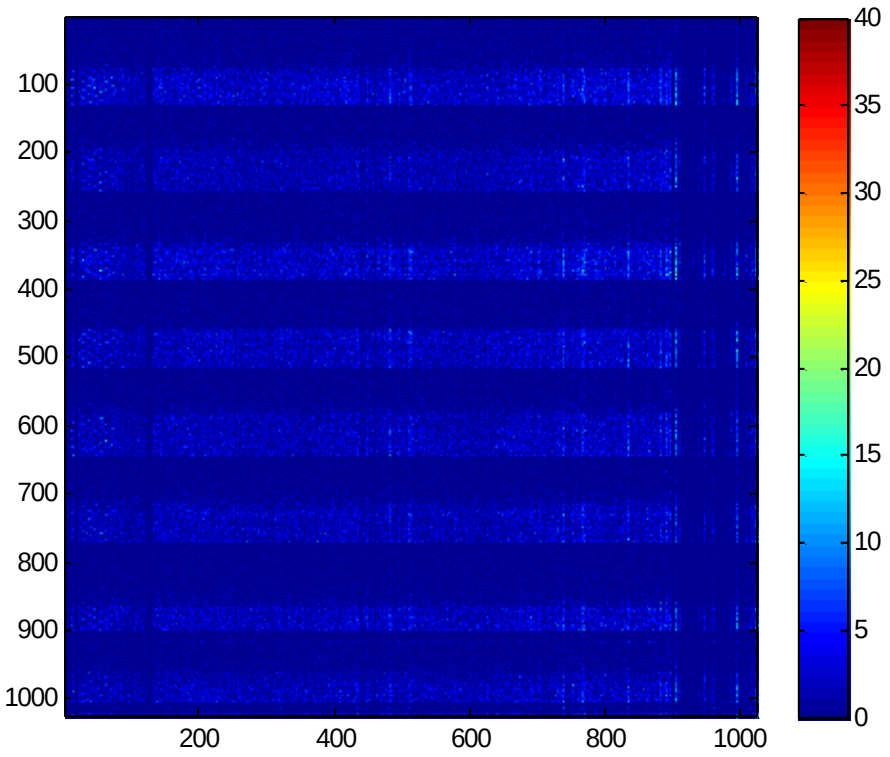

Figure 15. Flood scan of Si non-uniformity

To use this system in an imaging setting a reliable method to achieve a uniform detector response is required. There is a built in method to achieve this, it is possible to adjust threshold offset on a strip by strip basis and on a chip by chip basis. These adjustments affect what the strip threshold is relative to the global threshold on each side. This process is a very difficult process since adjusting of any of these values has a large up stream effect. Adjusting a strip threshold affects not only the strip but also both the chip threshold and the global threshold. Even with these challenges it is possible to adjust these values to achieve a uniform detector response in many ways; it is even possible to do this by hand; however this process is extremely time consuming.

To achieve the desired uniform response it was attempted to map the response of each strip as a function of the Global threshold.

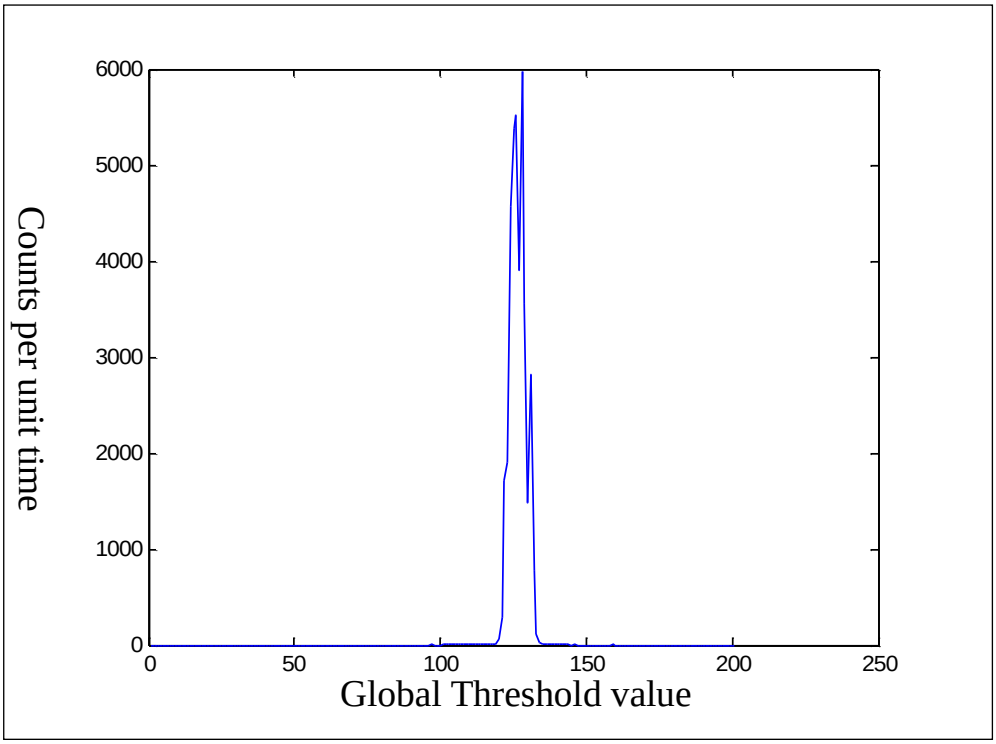

Figure 16. Si response vs global threshold

This was done by disabling all strips but a single one and then collecting data at a large percentage of all possible global threshold values (Figure 16). This maps the response of a strip and shows to what threshold value each strip wants to be at. With knowledge of how the offsets affect the strips from the global threshold, it allows for all strips to be adjusted to a uniform response. This requires a length of time that makes it unfeasible. So to speed up the collection of this data, instead of collecting on a strip by strip basis, this is done on a chip by chip level. The way the non-uniformity affects a strip means that this is just as good of a collection method as a single strip. The reason for this is that the noise floor tends to increase with strip on a chip and collection is done from strip 1 to 1024, meaning that the noise floor on a strip will not drown out actual counts on a previous strip.

In order to adjust all the values two scans must be taken per side, one with no source and one with a source. The scan without a source identifies the noise floor for each strip, this is then removed from the scan with a source (Figure 17). Since this is only to identify the noise floor and no real counts are collected the dwell time at any one threshold value is extremely small, as low as 5 ms. Once the response for all strips is collected it is then smoothed to remove noise (Figure 17). A desired count rate is chosen and then strip threshold maps are adjusted so all strips will have uniform count rates. This is done using some simple mathematics of finding the average threshold and finding the offset from this of every strip. It becomes an easy problem to adjust all the needed thresholds. All one needs is knowledge on how a change at each level affects that level and all preceding levels, this is a simple thing to figure out and needs to be done once per detector side. Using the same idea as before, it is possible to map the

response of a strip and then adjust a threshold and map the change in the response. With a map of how changes in the strip thresholds affect all other thresholds it becomes a simple problem to generate the new threshold tables.

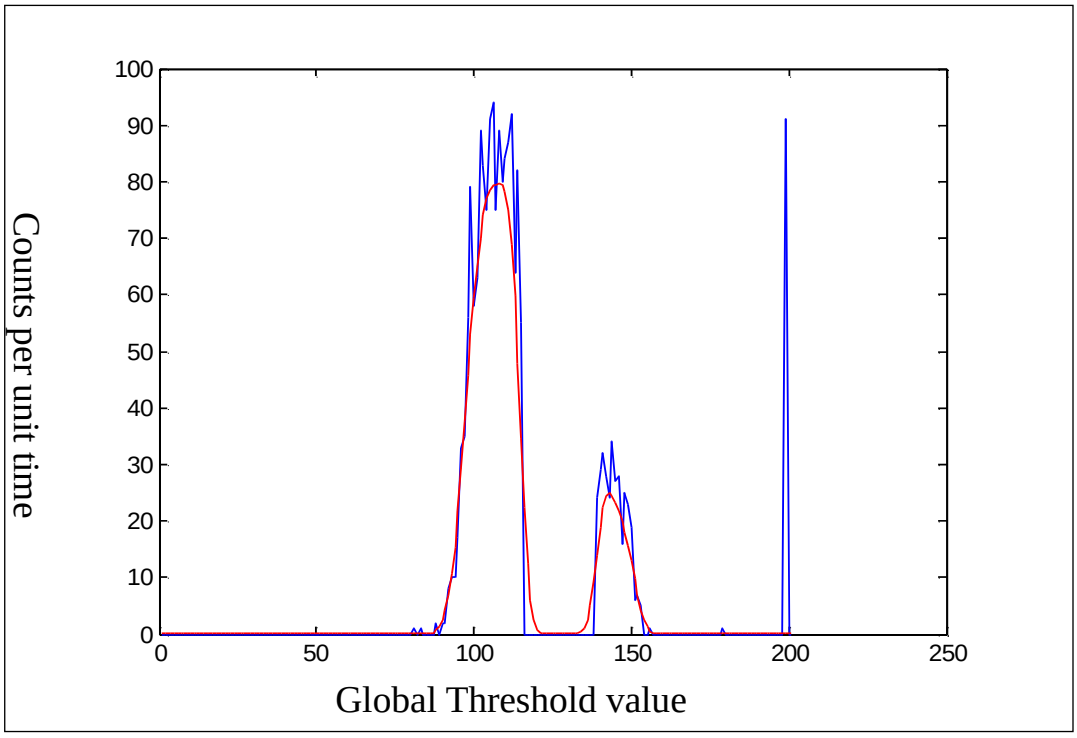

Figure 17. Si response of source with noise channels removed vs global threshold (original and smoothed)

This process seems time consuming but is relatively quick. The final fact that makes this procedure relatively quick is that it is quite easy to narrow the window of threshold values to scan over since the response tends to be confined to a few dozen values at most. With all this taken into account the whole process can be achieved in approximately an hour's worth of time. However some strips will still not behave as intended and might have to be adjusted by hand or disabled. The amount of these strips tends to be low or is populated by strips that are known to have greatly different

responses, high amount of noise or less signal, than others and can be remembered so as to not need to disable again.

CHAPTER VI

EVALUATION OF DUEL ENERGY SPECT CAMERA

Once the Si detector enclosure was manufactured the surfaces of the assembly that make contact with the Si detector were lapped in order to achieve the highest possible heat transfer. The detector was tested in a test enclosure before being placed inside the new detector enclosure in order to test the detector on a known system before placing in the new one. Once the initial testing was performed on the detector it was placed inside the newly designed enclosure and attached to the front of the HPGe detector. Once the system was assembled, ^{123}I was ordered in order to show that both detectors could collect data from the same source using different emitted energy photons. A syringe filled with ^{123}I was placed in front of a single pinhole collimator attached to the camera. Due to longer than anticipated time necessary in order to tune certain gain parameters on the Si detector and the half-life of ^{123}I, it was not possible to run a uniformity correction on the Si detector for this test.

One side of the Si detector seemed to not be responding correctly during the ^{123}I collection. Due to this the performance was evaluated on a single side level. This still allowed for the comparison of the measured response to simulations to assess properties such as focal lengths of both detectors and centers of field of view. Before the collection scan the stability of the Si detector was checked by collection of two flood images with a wait between of ~2 hours while the ^{123}I syringe scan was prepared. Based on visual inspection the detector did not have any apparent instability between scans, no strips seemed to loose count rate or gain count rate relative to baseline,

which suggests that the temperature was relatively stable. The collection to demonstrate the functionality of the camera utilized ~0.5 mCi of ^{123}I positioned 7cm in front of collimator (Figure 18).

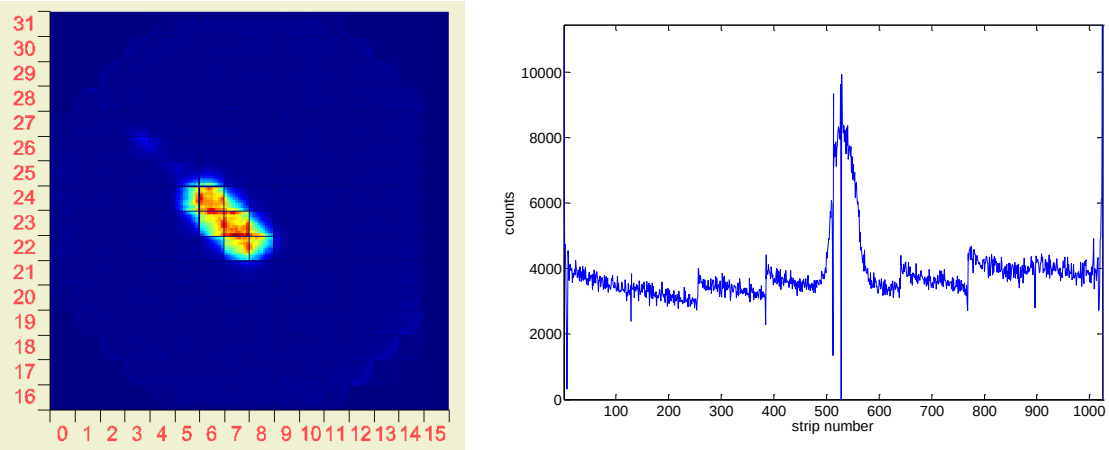

Figure 18. HPGE and Si projections of syringe

In order to test if this data is what is expected a simulation was run, the same as for multi-pinhole design, to compare expected results and collected data. The simulated data assumed that the syringe was 10mmX10mmX10mm, although this was not complete accurate due to the thickness of the wall of the syringe and the ends were not flat but concave. The simulation also assumed a centered object, which was not the case in the collected data making some shifting necessary to compare data. When comparing simulated vs. collected for the Si the data seems to be in relatively good agreement (Figure 19).

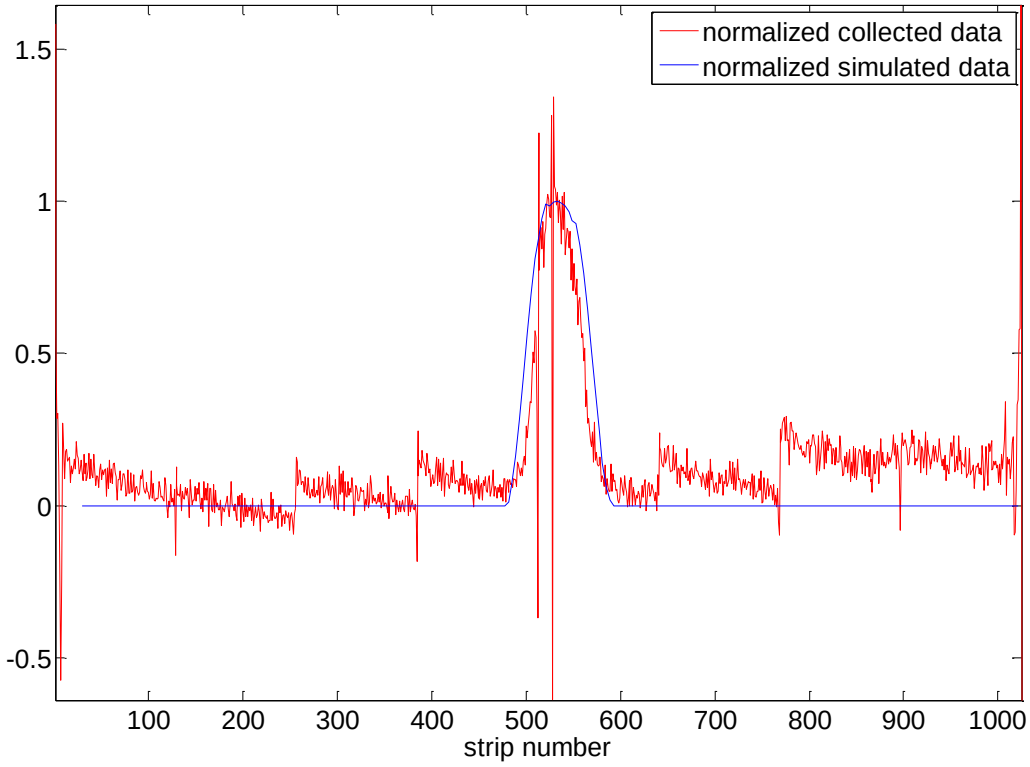

Figure 19. Comparison of Si Simulation vs. collected

The difference in the data is caused by the thickness of the syringe walls which were not included in the simulation. When comparing simulated vs. collected for the HPGe the data is in less agreement due to not fully accounting for the thickness of the syringe. The model also assumes flat walls while the syringe iss slightly concave at each end (Figure 20). The HPGe detector is rotated 45 degrees between the physical setup and simulations; this is due to the fact that the HPGe detector strips are rotated 45 degrees. However the results are close enough for us to be confident that the focal length is close to what we thought it was. This simulation has confirmed that we are indeed imaging ^{123}I with the 159 keV photon detected by the HPGe detector and the ~30 keV

photons by the Si detector. Both detectors also are collecting at different magnifications through the same pinhole. To our knowledge, this is the first time simultaneous imaging has been done of two photon energies at two different magnifications through a common collimator.

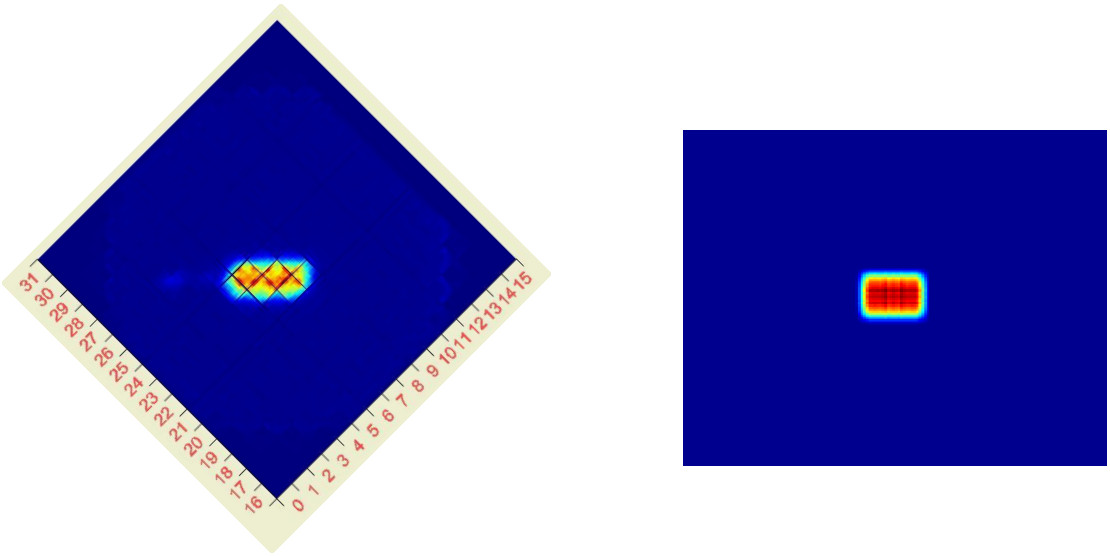

Figure 20. Comparison of HPGe simulation vs. collected

CHAPTER VII

MULTI-PINHOLE DESIGN FOR SYNTHETIC COLLIMATION DETECTOR

Once the system was designed the next task was to design a dedicated multi-pinhole collimator for the system, since the purpose of the system is to improve image reconstruction through the use of synthetic collimation, which is only possible in a multi-pinhole system. This requires a method of evaluating collimator designs by mapping how object space, for this system a 20x20x20mm^3 cylinder, projects through a collimator onto detector space (Figure 21). This is normally done using one of two different methods, Monte Carlo simulations or analytical calculations.

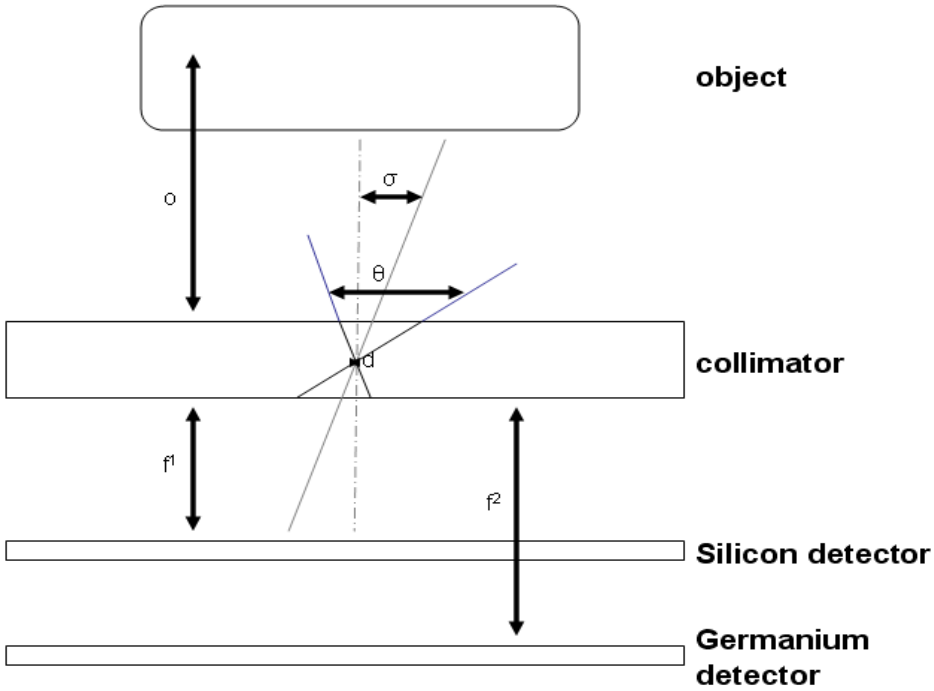

Figure 21. Set up of computation model

Monte Carlo simulations provide a complete idea of the system and work through modeling every photon and its interactions with the object and system. These simulations are extremely time consuming and would make evaluating a large amount of designs computationally extremely expensive. Analytical calculations of the collimator are much less computationally expensive but only give what might be considered a first order approximation. They, however, allow for a quick comparison of many collimator designs, making it ideal for our needs. There are many analytical methods for modeling SPECT systems, the method that we chose goes through each voxel in object space and then mathematically projects its activity through each pinhole onto detector space.

By evaluating collimator designs analytically, it is possible to quickly compare designs. After some preliminary investigations on different pinhole designs it was decided that a narrow design focus must be used. The reason for this is the extensive size of parameter space to search. With this in regard we evaluated a number of multi-pinhole configurations. After looking through many different pinhole layouts a four pinhole design based on the work of Christian Lackas was chosen (Figure 22) [64]. The reason for settling on this design is that it allows for maximum sampling of the object space while allowing for only minimal areas of more than double overlap, areas where photons could have come through any of more than 2 pinholes.

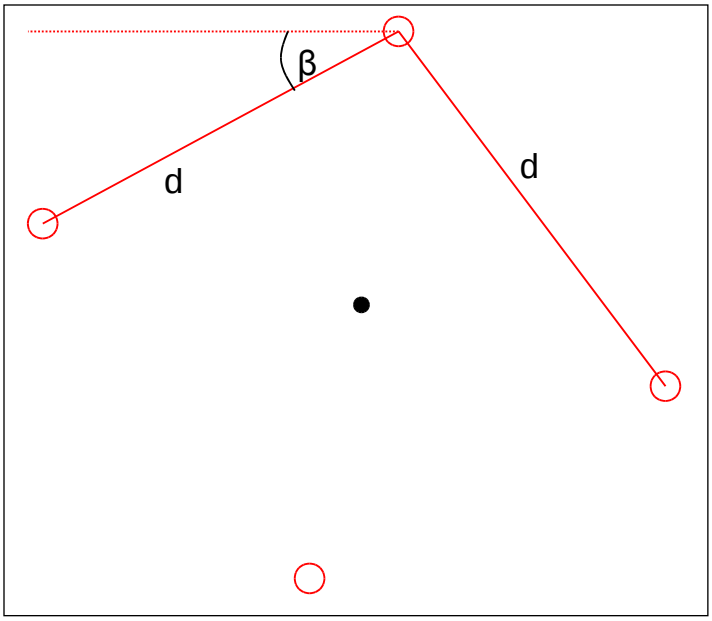

Figure 22. 4 pinhole design by Christian Lackas [64]

While designs with a central pinhole presented many benefits the higher degree of multiplexing was a concern for a first pinhole design. However, such designs might be considered for future collimators.

The design that was optimized was based on the 4 pinhole design mentioned above. It differed from the design by Christian Lackas by having the distance from center of the top and bottom pinholes different from that of the right and left pinholes (Figure 23). The reason for this is that the system will be used to image the mouse brain, an object that is more cylindrical in nature than spherical.

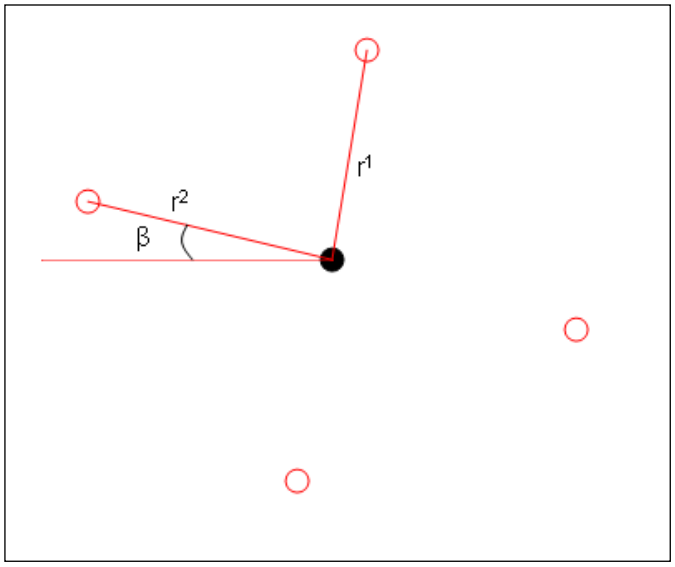

Figure 23. Modified 4 pinhole design

This allows for a narrowing of the field of view in one dimension and an extension in the other, and this produces projections that are elongated towards the top right and bottom left corners (Figure 24). Once a design was decided upon the next step was to look at a parameter range over which to limit our search.

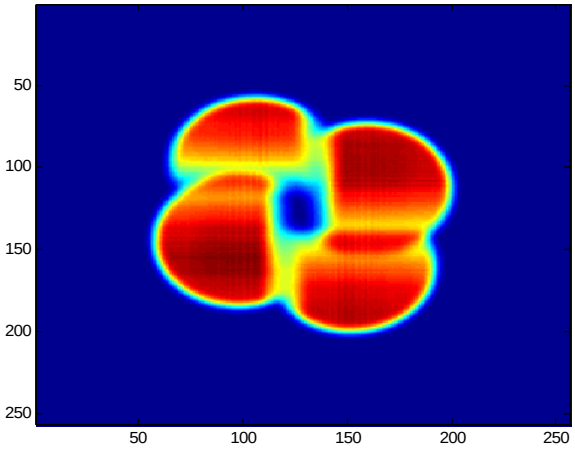

Figure 24. Projection of Modified 4 pinhole design on Si detector

β	Pinhole location tilt in collimator plane	**Fixed**
r1	Pinhole distance axis 1	**Variable**
r2	Pinhole distance axis 2	**Variable**
d	Pinhole diameter	**Fixed**
Θ	Opening angle of pinhole	**Variable**
σ	Pinhole tilt for viewing object space	**Variable**
o	Distance to center of object	**Variable**
f1	Focal length of Si detector	**Fixed**
f2	Focal length of HPGe detector	**Fixed**

Table 3. Simulation Parameters

Many of the parameters (table 3) were limited in the range over which they were allowed to vary, since having a situation where all pinholes are placed close to the center or having them pointing away from the object would be very unbeneficial. The degree of uniformity, as assessed by the standard deviation of sensitivity across the detectors and object, was decided as the defining metric for comparing collimator designs. There are two reasons for this, the first being that by limiting the parameter space we have already selected an area of relatively high sensitivity to search, the second being that this would naturally create a preferable amount of multiplexing. To compare two designs we calculated the standard deviation of the sensitivity of both detectors and object and then summed this together to create a single defining value for a collimator design.

The next question was how to find an optimized design as defined by our metric within our parameter space, searching the entire parameter space would prove to be an extremely computationally restrictive task. So a method of gradient descent was decided upon, a random initial seed is chosen in the defined parameter space and iteration by iteration these values are improved. This was done by selecting a parameter at random, changing it slightly to see how this changed the collimator based on the previously explained value, giving us a gradient to adjust this parameter on. This was done over and over again until one of two things happened: either the metric did not change over a certain amount of iterations, 10-20, or a fixed time expired, in order to stop a back and forth movements near a minimum. If time had expired, it was possible to check the value of the metric as a function of iteration to check conversion. If the optimization was judged to not be complete it is possible to restart we previous results as initial seed. This method allows for relatively quick local optimizations of different collimator designs. After Multi-hour run, Pinhole parameters began to converge to a set of uninteresting values with tiny opening angle (Table 4).

	MIN	MAX	Initial	Final
B	26.6deg	26.6deg	26.6deg	26.6deg
r1	5mm	10mm	6mm	6.1171mm
r2	7mm	14mm	8mm	7.7566mm
D	1mm	1mm	1mm	1mm
Θ	0deg	0deg	0deg	0deg
Σ	5deg	40deg	25deg	5.65509344deg
O	25mm	45mm	30mm	29.3862mm
f1	37mm	37mm	37mm	37mm
f2	85mm	85mm	85mm	85mm

Table 4. Simulation limits, seed, and output

The reason for the conversion to a uninteresting collimator design is that the comparison metric seems to prefer very small opening angles. A weighting based on sensitivity might be required since this would help to no longer have a preference for small opening angle. One attempt that seemed to produce a good result was using percentage of non-zero detector pixels divided by standard deviation as the metric for comparing collimator designs. When this new metric was used and the gradient descent method was used, more reasonable pinhole collimator parameters were produced (Table 5). When looking at the projections these resulting parameter values produce they are much more desirable compared to the initial seed (Figure 25). The reason the new projections are better are that large amounts of detector are used, along with the minimized multiplexing on Si detector, while maintaining high multiplexing on the HPGe detector and overall more uniform response.

	MIN	MAX	Initial	Final
B	26.6deg	26.6deg	26.6deg	26.6deg
r1	5mm	10mm	6mm	6.8968mm
r2	7mm	14mm	8mm	9.3806mm
D	1mm	1mm	1mm	1mm
Θ	0deg	0deg	0deg	0deg
Σ	5deg	40deg	11.5deg	14.6963674 deg
O	25mm	45mm	30mm	32.8106mm
f1	37mm	37mm	37mm	37mm
f2	85mm	85mm	85mm	85mm

Table 5. Simulation limits, seed, and output for new comparison metric

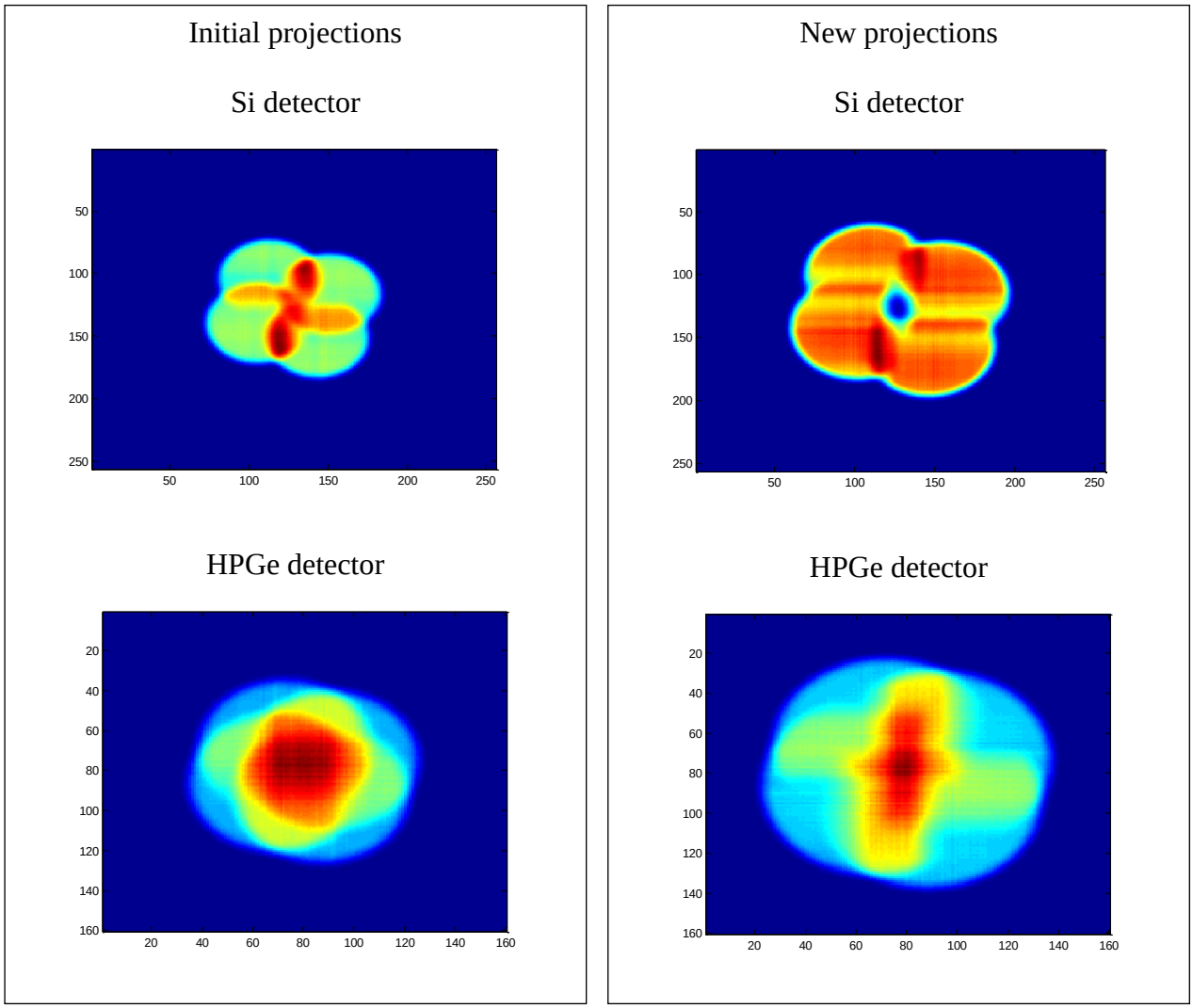

Figure 25. Projection of Modified 4 pinhole design using seed parameters and output from Table 5

CHAPTER VIII

CONCLUSION

A synthetic collimation camera using two different types of detectors is an important development for preclinical SPECT imaging. By inventing new and novel methods we have tried to overcome the traditional tradeoff of high resolution vs high sensitivity. By utilizing different types of detectors it is possible to overcome one problem with a previous synthetic collimation camera, SiliSPECT [65 66], that the rear detector in the camera had much lower sensitivity due to the interaction of the front detector with the photons the rear detector would otherwise detect.

The construction of this camera presented many challenges that needed to be overcome, and was only possible with recent advancements in detector design. The construction of the enclosure for the Si detector presented many challenges that had to be overcome from light seal issues, to making sure the detector was isolated from vibrations of the HPGe mechanical cooling system. Once an enclosure was designed, all the necessary steps needed to test and integrate with the existing detector represented a time consuming process. The need for a dedicated collimator designed to take full advantage of this system presents an area of huge potential. The proper collimator will be able to make full use of this system, however the infinite amount of possibilities makes finding this collimator design a daunting task.

The development of methods for image reconstruction that utilize both detectors to the maximum is still a large area of interest. The potential of such a camera in a SPECT system for mouse brain image is huge. The ability to have extremely high

spatial resolution, high scatter rejection and high sensitivity is an extremely exciting proposition. Once this system is fully operational it should allow for new and interesting views of radiotracer distribution in the mouse brain or objects of roughly the same size.

REFERENCES

1. Mankoff DA. A definition of molecular imaging. *J Nucl Med*.2007;48:18N, 21N.

2. Cherry SR. In vivo molecular and genomic imaging: new challenges for imaging physics. *Phys Med Biol*. 2004;49:R13–48.

3. Bailey DL, Karp JS, Surti S. Physics and instrumentation in PET, in positron emission tomography: basic science and clinical practice. Philadelphia: Springer; 2003. p. 41–67.

4. Ishizu K, Mukai T, Yonekura Y, Pagani M, Fujita T, Magata Y, et al. Ultra-high resolution SPECT system using four pinhole collimators for small animal studies. *J Nucl Med*. 1995;36:2282–7.

5. Jaszczak RJ, Li J, Wang H, Zalutsky MR, Coleman RE. Pinhole collimation for ultra-high-resolution, small-field-of-view SPECT. *Phys Med Biol*. 1994;39:425–37.

6. McElroy DP, MacDonald LR, Beekman FJ, Yuchuan Wang, Patt BE, Iwanczyk JS, et al. Evaluation of A-SPECT: a desktop pinhole SPECT system for small animal imaging. *Nuclear Science Symposium Conference Record*, 2001 IEEE, vol. 3, pp. 1835–1839, 2001. doi:10.1109/NSSMIC.2001.1008699.

7. Weber DA, Ivanovic M, Franceschi D, Strand SE, Erlandsson K, Franceschi M, et al. Pinhole SPECT: an approach to in vivo high resolution SPECT imaging in small laboratory animals. *J Nucl Med*. 1994;35:342–8.

8. Beekman FJ, Vastenhouw B. Design and simulation of a highresolution stationary SPECT system for small animals. *Phys Med Biol*. 2004;49:4579–92.

9. Beekman FJ, van der Have F, Vastenhouw B, van der Linden AJA, van Rijk PP, Burbach JPH, et al. U-SPECT-I: a novel system for submillimeter-resolution tomography with radiolabeled molecules in mice. *J Nucl Med*. 2005;46:1194–200.

10. Wilson DW, Barrett HH, Furenlid LR. A new design for a SPECT small-animal imager. *Nuclear Science Symposium Conference Record, 2001* IEEE, vol. 3, pp. 1826–1829, 2001.doi:10.1109/ NSSMIC.2001.1008697.

11. Meikle SR, Kench P, Weisenberger AG, Wojcik R, Smith MF, Majewski S, et al.Aprototype coded aperture detector for small animal SPECT. *Nuclear Science Symposium Conference Record*, 2001 IEEE, vol. 3, pp. 1580–1584, 2001.doi:10.1109/NSSMIC.2001.1008641.

12. Liu Z, Kastis GA, Stevenson GD, Barrett HH, Furenlid LR, Kupinski MA, et al. Quantitative analysis of acute myocardial infarct in rat hearts with ischemia-reperfusion using a highresolution stationary SPECT system. *J Nucl Med.* 2002;43:933–9.

13. Rowe RK, Aarsvold JN, Barrett HH, Chen JC, Klein WP, Moore BA, et al. A stationary hemispherical SPECT imager for 3-dimensional brain imaging. *J Nucl Med*. 1993;34:474–80.

14. Schramm NU, Ebel G, Engeland U, Schurrat T, Behe M, Behr TM. High-resolution SPECT using multipinhole collimation. *IEEE Trans Nucl Sci*. 2003;50:315–20.

15. Lackas C, Schramm NU, Hoppin JW, Engeland U, Wirrwar A, Halling H. T-SPECT: a novel imaging technique for small animal research. IEEE Trans Nucl Sci. 2005;52:181–7.

16. Kim H, Furenlid LR, Crawford MJ, Wilson DW, Barber HB, Peterson TE, et al. SemiSPECT: a small-animal single-photon emission computed tomography (SPECT) imager based on eight cadmium zinc telluride (CZT) detector arrays. *Med Phys*. 2006;33:465–74.

17. Miller BW, Furenlid LR, Moore SK, Barber HB, Nagarkar VV, Barrett HH. System Integration of FastSPECT III, a Dedicated SPECT Rodent-Brain Imager Based on BazookaSPECT Detector Technology. *IEEE Nucl Sci Symp Conf Rec* (1997) 2009, Oct. 24 2009-Nov. 1 2009;4004–4008.

18. Beekman F, van der Have F. The pinhole: gateway to ultra-highresolution three-dimensional radionuclide imaging. *Eur J Nucl Med Mol Imaging*. 2007;34:151–61.

19. Wu C, de Jong JR, van Andel HA G, van der Have F, Vastenhouw B, Laverman P, et al. Quantitative multi-pinhole small-animal SPECT: uniform versus non-uniform Chang attenuation correction. *Phys Med Biol.* 2011;56:N183–93.

20. Constantinesco A, Choquet P, Monassier L, Israel-Jost V, Mertz L. Assessment of left ventricular perfusion, volumes, and motion in mice using pinhole gated SPECT. *J Nucl Med.* 2005;46:1005–11.

21. Golestani R, Wu C, Tio RA, Zeebregts CJ, Petrov AD, Beekman FJ, et al. Small-animal SPECT and SPECT/CT: application in cardiovascular research. *Eur J Nucl Med Mol Imaging*. 2010;37:1766–77.

22. Auricchio A, Acton PD, Hildinger M, Louboutin JP, Plossl K, O'Connor E, et al. In vivo quantitative noninvasive imaging of Eur J Nucl Med Mol Imaging gene transfer by single-photon emission computerized tomography. *Hum Gene Ther*. 2003;14:255–61.

23. Kumar SR, Deutscher SL, Figueroa SD. Tumor targeting and SPECT imaging properties of an (111)In-labeled galectin-3 binding peptide in prostate carcinoma. *Nucl Med Biol.* 2009;36:137–46.

24. Gambini JP, Cabral P, Alonso O, Savio E, Figueroa SD, Zhang X, et al. Evaluation of 99mTc-glucarate as a breast cancer imaging agent in a xenograft animal model. *Nucl Med Biol*. 2011;38:255–60.

25. Luo SN, Wang Y, Lin JG, Qiu L, Cheng W, Zhai HZ, et al. Animal studies of (99m)Tc-i-PIDP: a new bone imaging agent. *Appl Radiat Isotopes*. 2011;69:1169–75.

26. Booij J, de Bruin K, de Win MML, Lavini C, den Heeten GJ, Habraken JBA. Imaging of striatal dopamine transporters in rat brain with single pinhole SPECT and co-aligned MRI is highly reproducible. *Nucl Med Biol*. 2003;30:643–9.

27. Bennink RJ, Hamann J, de Bruin K, ten Kate FJ, van Deventer SJ, te Velde AA. Dedicated pinhole SPECT of intestinal neutrophil recruitment in a mouse model of dextran sulfate sodium-induced colitis. *J Nucl Med*. 2005;46:526–31.

28. Goorden MC, Beekman FJ. High-resolution tomography of positron emitters with clustered pinhole SPECT. Phys Med Biol. 2010;55:1265–77.

29. van der Have F, Vastenhouw B, Rentmeester M, Beekman FJ. System calibration and statistical image reconstruction for ultrahigh resolution stationary pinhole SPECT. *IEEE Trans Med Imaging.* 2008;27:960–71.

30. Miller BW, Van Holen R, Barrett H, Furenlid L. A system calibration and fast iterative reconstruction method for next-generation SPECT imagers. *IEEE Trans Nucl Sci.* 2012;59:1990–6.

31. Branderhorst W, Vastenhouw B, van der Have F, Blezer ELA, Bleeker WK, Beekman FJ. Targeted multi-pinhole SPECT. Eur *J Nucl Med Mol Imaging*. 2011;38:552–61.

32. Mok GS, Tsui BM, Beekman FJ. The effects of object activity distribution on multiplexing multi-pinhole SPECT. *Phys Med Biol*. 2011;56:2635–50.

33. Vunckx K, Suetens P, Nuyts J. Effect of overlapping projections on reconstruction image quality in multipinhole SPECT. *IEEE Trans Med Imaging*. 2008;27:972–83.

34. Cherry SR, Sorensen J, Phelps ME. *Physics in nuclear medicine*. Philadelphia: Saunders; 2012

35. kim YJ, Ichise M, Ballinger JR, et al. Combination of dopamine transporter and D2 receptor SPECT in the diagnostic evaluation of PD, MSA, and PSP. Mov Disord. 2002; 17: 303–312.

36. Amman M and Luke P N.Three-dimensional position sensing and field shaping in orthogonal-strip germanium gamma-ray detectors *Nucl. Instrum. Methods Phys. Res. 2000;* A 452 155–66

37. Blair J, Beckedahl D, Kammeraad J and Schmid G. Spatial resolution attainable in germanium detectors by pulse shape analysis *Nucl. Instrum. Methods Phys. Res.* A. 1999; 422 331–6

38. Burks M, Jordan E, Hull E, Mihailescu L and Vetter K. Signal interpolation in germanium detectors for improved 3D position resolution *IEEE Nuclear Science Symp. Conf. Record, 2004* vol 2. *2004* pp 1114–8

39. Chen C L, Wang Y, Lee J J and Tsui B M. Toward quantitative small animal pinhole SPECT: assessment of quantitation accuracy prior to image compensations *Mol. Imaging Biol. 2009;* 11 195–203

40. Cooper R J *et a.* SmartPET: applying HPGe and pulse shape analysis to small-animal PET *Nucl. Instrum. Methods Phys. Res.* A. 2007; 579 313–7

41. Gros S, Hammond N J, Lister C J, Chowdhury P, Fischer S M and Freeman S J. Performance tests of large area position-sensitive planar germanium detectors with conventional and amorphous contacts *Nucl. Instrum. Methods Phys. Res.* A. 2009; 602 467–76

42. Hansen W L and Haller E E. Amorphous germanium as an electron or hole blocking contact on high-purity germanium detectors *IEEE Trans. Nucl. Sci. 1977;* 24 61–3

43. Hasegawa B H, Stebler B, Rutt B K, Martinez A, Gingold E L, Barker C S, Faulkner K G, Cann C E and Boyd D P. A prototype high-purity germanium detector system with fast photon-counting circuitry for medical imaging *Med. Phys. 1991;* 18 900–9

44. Hayward J and Wehe D. Incomplete charge collection in an HPGe double-sided strip detector *Nucl. Instrum. Methods Phys. Res.* A. 2008; 586 215–23

45. Hayward J P and Wehe D K. Charge loss correction in a high-purity germanium double-sided strip detector *IEEE Trans. Nucl. Sci. 2008;* 55 2789–97

46. Hayward J P and Wehe D K. Inter-strip interpolation measurements in a high-purity germanium double-sided strip detector *IEEE Trans. Nucl. Sci. 2009;* 56 800–7

47. Hutton B F, Buvat I and Beekman F. Review and current status of SPECT scatter correction *Phys. Med. Biol. 2011;* 56 R85

48. Hwang A B, Franc B L, Gullberg G T and Hasegawa B. Assessment of the sources of error affecting the quantitative accuracy of SPECT imaging in small animals *Phys. Med. Biol. 2008;* 53 2233–52

49. Kuikka J T, Tenhunen-Eskelinen M, Jurvelin J and Kiili¨anen. Physical performance of the Siemens MultiSPECT 3 gamma camera *Nucl. Med. Commun. 1993;* 14 490–7

50. Luke P N, Amman M, Phlips B F, Johnson W N and Kroeger R A. Germanium orthogonal strip detectors with amorphous-semiconductor contacts *IEEE Trans. Nucl. Sci. 2000 ;* 47 1360–3

51. Luke P N, Cork C P, Madden N W, Rossington C S and Wesela M F, Amorphous Ge bipolar blocking contacts on Ge detectors *IEEE Trans. Nucl. Sci. 1992;* 39 590–4

52. McCready V R, Parker R P, Gunnersen E M, Ellis R, Moss E, GoreWG and Bell J. Clinical tests on a prototype semiconductor gamma-camera *Br. J. Radiol. 1971;* 44 58–62

53. Mueller B, O'Connor M K, Blevis I, Rhodes D J, Smith R, Collins D A and Phillips S. Evaluation of a small cadmium zinc telluride detector for scintimammography *J. Nucl. Med. 2003;* 44 602–9

54. Phlips B F, Johnson W N, Kroeger R A, Kurfess J D, Phillips G, Wulf E A and Luke P N. Development of germanium strip detectors for environmental remediation *IEEE Trans. Nucl. Sci. 2002;* 49 597–600

55. Vanhove C, Defrise M, BossuytAand Lahoutte T. Improved quantification in single-pinhole and multiple-pinhole SPECT using micro-CT information *Eur. J. Nucl. Med. Mol. Imaging. 2009;* 36 1049–63

56. Vetter K, BurksMandMihailescu L. Gamma-ray imaging with position-sensitive HPGe detectors *Nucl. Instrum. Methods Phys. Res.* A. 2004; 525 322–7

57. Wulf E A, Ampe J, JohnsonWN, Kroeger R A, Kurfess J D and Phlips B E. Depth measurement in a germanium strip detector *IEEE Trans. Nucl. Sci. 2002* 49 1876–80

58. Wulf E A, Phlips B F, Johnson W N, Kroeger R A, Kurfess J D and Novikova E I. Germanium strip detector Compton telescope using three-dimensional readout *IEEE Trans. Nucl. Sci*. 2003; 50 1182–9

59. Johnson LC, Ovchinnikov OS, Peterson TE – Characterization of a Small-Animal High-Purity Germanium SPECT System – IEEE Nuclear Science

Symposium and Medical Imaging Conference (NSS/MIC) 2012, pp. 2569 – 2575

60. Shepp LA, Vardi Y. Maximum likelihood reconstruction for emission tomography. IEEE Trans Med Imaging. 1982; MI-1:113–122.

61. Lange K, Carson R. EM reconstruction algorithms for emission and transmission tomography. J Comput Assist Tomogr. 1984; 8:306–316.

62. Dempster A, Laird N, Rubin D. Maximum likelihood from incomplete data via the EM algorithm. *J R Stat Soc* [B]. 1977; 39:1–38.

63. Kaufman L. Implementing and accelerating the EM algorithm for positron emission tomography. *IEEE Trans Med Imaging*. 1987; MI-6:37–51.

64. Kaufman L. Maximum likelihood, least squares and penalized least squares for PET. *IEEE Trans Med Imaging*. 1993;12:200–214.

65. Lackas C, 2006, : Design and Implementation of a High-Resolution and High-Sensitivity Small-Animal SPECT Imaging System. PhD dissertation, Jülich : Forschungszentrum Jülich, 2006, Techn. Hochsch., Diss.--Aachen, 2005 (9783893364510)

66. Shokouhi S, Metzler SD, Wilson DW, Peterson TE. Multi-pinhole collimator design for small-object imaging with SiliSPECT: a high-resolution SPECT. *Phys. Med. Biol*. 2009; 454:207–225.

67. Shokouhi S, Wilson DW, Metzler SD, Peterson TE. Evaluation of image reconstruction for mouse brain imaging with synthetic collimation from highly multiplexed SiliSPECT projections. *Phys Med Biol*. 2010;55:5151–5168.